ITEA-2018-17030
DayTiMe

Digital Lifecycle Twins for Predictive Maintenance

Deliverable: D2.1 State-of-the-Art on use cases and enabling technologies

Due date of deliverable: (31-10-2019)
Actual submission date: (19-02-2020)

Start date of Project: 01 Oct 2019 Duration: 42 months

Responsible WP2: Philips

Revision: proposed

Dissemination level		
PU	Public	✓
PP	Restricted to other programme participants (including the Commission Service	
RE	Restricted to a group specified by the consortium (including the Commission Services)	
CO	Confidential, only for members of the consortium (excluding the Commission Services)	

0 DOCUMENT INFO

Author

Author	Company	E-mail
Krelis Blom	PMS	krelis.blom@philips.com
Eelco Galestien	PCL	eelco.galestien@philips.com
Mustafa Aydin	Siemeks	mustafa.aydin@triatech.com.tr
David Verstraeten	Yazzoom	david.verstraeten@yazzoom.com
Qi Gao	PEN	q.gao@philips.com
Roberto Rocchetta	TU/e	rocchetta@tue.nl
Zehra Cataltepe	Tazi	zehra@tazi.ai
Jaap van Etten	Datenna	jaap@datenna.com
Pim van der Meulen	Target Holding	pim.van.der.meulen@target-holding.nl
Ipek Dursun	TU/e	i.dursun@tue.nl
Ajay Kottapalli	RUG	a.g.p.kottapalli@rug.nl
Martijn Liem	PS-Tech	martijn.liem@ps-tech.com

Documents history

Document version #	Date	Change
v0.1	11-12-2019	First draft
v0.2	17-12-2019	Feedback from internal reviewers and partners
Final	23-12-2019	Final version
2.0	19-02-2020	Public version

Document data

Editor Address data	Name: Qi Gao Partner: Philips Research Address: High Tech Campus 34, Phone: +31 681406401

Distribution list

Date	Issue	E-mailer
		AI_daytime_all@natlab.research.philips.com

Table of Contents

1 Executive summary

This deliverable provides an overview of the current state-of-the-art for the four use cases in the DayTime project.

Philips Consumer Lifestyle introduces the design challenge of smart rota shaver and will focus on the development of sensor solution and predictive models of skin-cutter distance.

Philips healthcare summarizes its maintenance process and the status of predictive model development for MRI system. The MRI use case will apply advanced data analytics and AI to improve the system diagnostics using data from various sources incl. device log, sensors and maintenance service records.

Yazzoom gives an overview of the industrial boiler system and focus on using AI on sensor data for anomaly detection and root-cause analysis.

Triatech presents the use case of medication and medical supply management system and will develop predictive models for its maintenance process. In addition, a set of enabling technologies will be applied across use cases.

A number of partners provide the state-of-the-art on these technologies including big data analytics (TU Eindhoven, Philips Research), machine learning (Tazi), natural language processing (Datenna), machine log data analysis (Target holding), predictive analytics and optimization (TU Eindhoven), sensor technology (University of Groningen), visualization and simulation (PS Tech).

2 State of the art on user cases

2.1 Use case: smart shaver

2.1.1 Introduction to Philips rota shaving

In comparison with other rota competitors, the balance between closeness and irritation of Philips Shavers is at a high level. That means that at the same level of closeness a Philips Shaver is irritating less than Chinese competitors or for example, Remington. Perhaps the most important element in the shaver is the cutting element, or shaving system. The shaving system, consisting of a cap and a cutter, changes significantly with every shaver generation to meet consumer needs and market trends.

Figure 1: Philips shaving head (S7000 series), showing the shaving systems and surrounding SkinGlide rings.

It works on the principle that the user does not have to steer a blade into cutting hairs, but that the skin is pushed in between the lamellae of the cap, lifting hair into the path of the cutter. Hair is cut between the cutting edges of the cutter and the lamellae. The skin bulges or 'domes' in between the lamella, further reducing the distance of the skin to the cutter. Getting the skin-cutter distance as small as possible will ensure the closest possible shave. However, if the skin protrudes too far into the shaving system the skin will be damaged by the cutter. This causes a burning sensation, irritation and, redness, and in the extreme case deeper cuts and bleeding. Skin-cutter distance is abbreviated to SCD from here on.

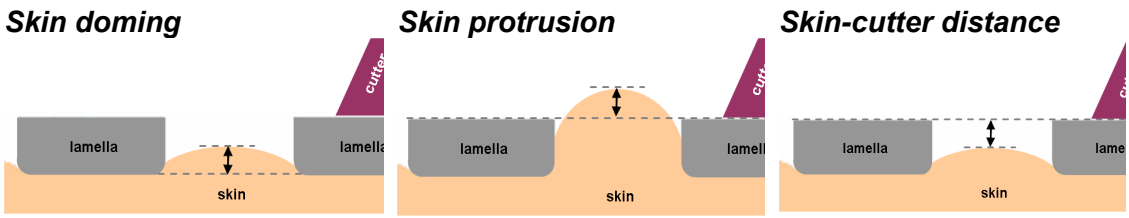

2.1.2 Current status and use case challenges

Rota shaving design challenges

As described in the introduction, the challenge is reducing the SCD to exactly zero, without overshooting. Too little skin doming means the hair isn't cut close to the skin, resulting in poor closeness. Too much skin doming means the skin is pushed into the path of the cutter, resulting in skin damage (irritation, burning sensation and/or redness)

This is complicated by the fact that the skin doming mechanism is an interaction between the skin physiology and the handling of the shaver, most dominantly the applied pressure and motion. The mechanical properties of skin vary between persons. Within a person the properties are also constantly changing with ambient conditions, age, lifestyle, etc.. The pressure exerted on the cap contributes to skin doming. However, not all users press with the same force. Furthermore, keeping a constant pressure while simultaneously moving over the skin proves difficult for most users.

Due to the viscoelastic properties of skin, the speed at which the cap moves over the skin also contributes to skin doming. Keeping the appliance stationary leads to the highest levels of skin doming as the skin relaxes into the slots. Lastly, there are many other factors that will likely influence the SCD, such as friction coefficients and skin roughness. The interactions are often difficult to investigate, and vary between individual users.

Current shavers are designed for the average skin physiology and try to steer the average SCD to zero. Since there is currently no real-time measurement of the SCD during a shave, the SCD is estimated through lab measurements on skin doming in vivo, objective measurements of hair length and skin irritation after a shave, and through test panels reporting on various attributes of the shaving process and result.

Because the current state of the art does not allow for adjustment of the SCD to changing conditions or different skin parameters, a lot of work goes into optimizing the geometry of the product to make the system less sensitive to these variations. A recent development is the Smart Shaver, which instructs the user on proper shaving motion, thus reducing user-handling variation (see State of the Art for a description of the Philips Smart Shaver).

Use-case goal

In this project, we will focus on development and we aim to end with a demonstrator that proves feasibility. Industrialization of the solutions found will not be in scope.

2.2 Use case: smart maintenance for MRI

2.2.1 Introduction to MRI

MRI (Magnetic Resonance Imaging) devices are used to create images of the inside body for diagnostic purposes. Referring physicians will base their diagnostic conclusion on the diagnostic images of the patient made by the MRI device.

Figure 1. Philips MRI system

A session where the patient is placed inside the MRI system is called an examination. A typical examination duration takes between 10 and 30 minutes. During the examination multiple scans are performed. Typically 5 to 10 scans per examination are performed. Each scan results in multiple images which can be experienced as slices through the body. Each scan has a different purpose. Scans differ to balance between time and resolution of the resulting images. As an example: the first scan of an examination is a Scout scan which is a fast low resolution scan to view a large part of the body enabling planning of the next high resolution scans on the right anatomy or clinical question. Scans also differ in technique to balance between robustness for patient motion during the scan and resolution or sharpness of the images. Techniques also differ in what needs to be shown depending on what the referring physician wants to see, e.g. the grey or white matter of the brain, flow of fluids, tissues like nerves and cancer cells. Scans are controlled by scan parameters which can be modified by the operator to optimize the scan for the diagnostic question. Hundreds of parameters are available to modify and optimize the scan. The operator typically modifies a few parameters to adapt the scan to the patient, obtaining the best image quality.

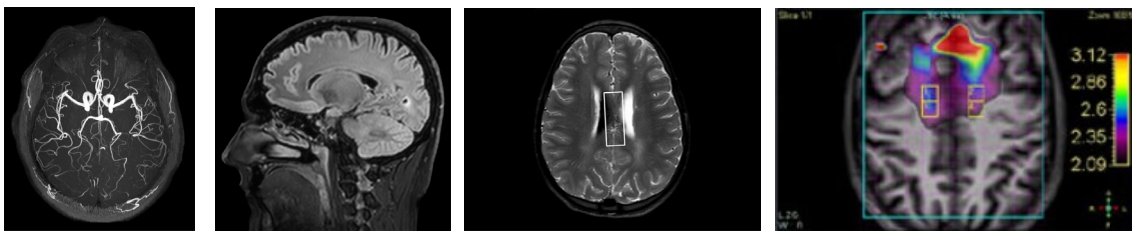

Figure 2. Examples of resulting MRI images using different scan techniques. From left to right: imaging blood vessels, imaging brain, imaging brain trauma, fMRI (functional MRI).

The MRI room setup is distributed over four rooms.
Patient Preparation Room

The operator prepares the patient before the patient is allowed to enter the examination room. Main activity is to ensure the patient does not have metal in clothing, make-up, jewelry or implants. Metal will have impact on the image quality and is safety related as well.

Examination Room

The patient is positioned by the operator in the magnet located in the Examination Room. The Examination Room is RF-shielded to prevent RF interference from outside impacting the image quality, and to keep RF generated signals by MRI equipment inside the room. The examination room size is tuned to prevent magnetic interaction with non-MRI equipment located outside the room. Inside the room only special equipment is allowed. Like special non-magnetic wheel chairs and infusion standards. MRI service engineers do have special titanium (non-magnetic) tools to service the equipment inside the examination room.

Operator Room

In the Operator Room the operator controls the MRI system. Scans are selected and adapted, and images viewed on quality.

Technical Room.

Control, power and cooling equipment for the MRI system is located in the technical room near the MRI examination room.

2.2.2 Current status and use case challenges

Maintenance process

Uptime is a critical KPI for MRI systems. Systems which run 24hrs / 7 days in the week are no exception anymore. Planned and remote predictive service are key elements in achieving those needs.

Planned maintenance

The activities performed during the maintenance are defined per configuration. They vary from re-adjusting to proactive cleaning filters.

Predictive maintenance

Majority of systems are connected and machine data is uploaded to a Philips Cloud. The machine data is used to monitor the systems under service contract. Alerts are created towards the service organization in case of degradation and predictive failures based on analysis of the available data

Corrective maintenance

In case of failures, a customer calls the helpdesk. The helpdesk will try to remotely diagnose the problem using uploaded machine data in combination with remotely triggered tests, executed locally at the MRI system.

Personas in the Maintenance process are:

Operator/Customer

Calls the helpdesk in case of issues.

Helps the Remote Service Engineer (RSE) in diagnosing the problem, by answering questions and perform boot and power actions on request of the RSE.

HelpDesk Engineer

Answers the call and delegates the investigation by submitting a Service Work Order (SWO). A SWO is a data record in which actions are consolidated between the moment of reporting the issue and solving the issue.

Remote Service Engineer (RSE)
Responsible to diagnose issues remotely triggered by an SWO. The RSE will capture his findings in the SWO and will close the SWO in case the issue could be solved remotely, or delegates the SWO to the local Field Service Engineer (FSE) for fixing the issue locally or perform further diagnostics locally in case remotely the root-cause could not be uniquely identified.
Field Service Engineer (FSE)
Responsible to locally maintain and fix the system. The FSE is the service person who replaces parts and perform local diagnosis
Remote Monitoring Engineer (RME)
Monitors connected systems globally. In case of alerts created by proactive models using machine data, the RME will create a SWO and dispatch the SWO with his findings to the local applicable market organization where the SWO will end at the RSE or FSE.

Model development

Models to support predictive service are built on top of collected machine data. Typical machine data consists of:
Configuration Data
Identifies the unique composition of the MRI system, with identifiers for all hardware elements and versions of the hardware
Logfiles
One central logfile across the complete MRI system contains in an unstructured way the workflow of the system including error events reported by hardware.
Sensor Data
Dedicated files per sensor property contain the sampled values of sensors
Test Data
Test results of tests executed at idle time and test results of tests triggered by FSE and RSE.

The collected data is transferred in structured data and loaded in a data warehouse. Algorithms are using the continuous stream of data and generate alerts which are inspected by RSE's.

ETL scripts are used to translate unstructured logfiles into structured data. When logfiles change, or new hardware is introduced, or new software workflows are defined, the ETL's will be adapted after which models will be inspected or updated to fulfill the need of proactive monitoring.

Alerts generated by models on top of machine data are evaluated by RME's. In case of false alerts the model development teams are informed, who will analyze the false alert and update the models where needed.

The Use Case for MRI systems in the context of Daytime is built around 3 challenges:

- In which extend can behavioral information be retrieved from logfiles without the need for ETL's
- Can enhanced AI techniques be used to monitor sensor data
- In which extend can textual data be used to validate proactive service models

2.3 Use case: industrial boilers

2.3.1 Introduction to industrial boilers

Industrial Boilers are direct-fired boilers designed and used to provide steam to industrial processes. They may use various type of fuels, liquid or gaseous, according to the application. An Industrial Boiler is generally made up of two major systems. One system is the fuel-air-flue gas system (fireside) and the other is the water-steam system (waterside). Heat is provided to convert water into steam.

- *Fuel-air-flue gas system*

In order to obtain high enough steam temperatures at low load, the boiler must run with a minimum number of burners in operation. The longer flame length will help to increase the temperature of the steam. When the boiler load is increased additional burners will start automatically.

The combustion air system consists of a combustion air damper and a combustion air fan which provide the requested amount of air according to specific sequences.

There is a main fuel control valve to maintain a constant pressure to the downstream burner system. The load signal is translated to control the individual burner control valves. The individual burner control valves are used to control the load

Flue gas recirculation (FGR) to burners allows for NOx control. The amount of FGR to burners is a ratio of the sum of the combustion air flow and the FGR to burners flow. The FGR to burners needs to be sucked into the combustion air duct. Therefore, a constant pressure needs to be upheld upstream the combustion air fan.

Flue gas recirculation (FGR) to boiler allows for a higher heat transfer. The amount of FGR to boiler is higher at low loads than at high loads. However, this FGR must remain in operation at every load to ensure the cooling of the expansion joint.

- *Water-steam system*

Water is introduced into a pressurized drum to be converted into steam. The pressure drum level must be properly controlled within certain limits. The produced steam is led into a steam drum header and send to a superheater to produce superheated steam when required.

2.3.2 Current status and use case challenges

Sensor data are currently used to operate the boiler through the use of PLCs and SCADA. They are usually stored in a specific historian, but they are often not exploited for improving operation of the boiler. Anomalies are often detected too late or not detected at all. Historical data is then used for analysing the root-causes of the problem at hand.
Anomaly detection on the edge and/or on the cloud could deliver additional value to the industrials.

The Use Case for Industrial Boilers in the context of Daytime is built around the following challenges:

- To which extent can anomalies be detected using Artificial Intelligence based on sensor data?
- To which extent are additional sensors and data necessary to detect anomalies using Artificial Intelligence?
- To which extent can detected anomalies be related to specific root-causes and explained by the physics of the boilers?
- To which extent can anomaly detection be automated in order to alert and guide industrials to improve the usage of their boilers?

2.4 Use case: medication and medical supply management system

2.4.1 Introduction to medication and medical supply management system

The medication and medical supply management system (Stockart) Systems are used to manage in hospital's medication and medical supply. In order to meet the medication and medical supply needs of patients, begin process starting from the pharmacy/warehouse to dispatching to the service points and ending with the using for the patient. There is a risk of health and high cost loss due to medication and medical supply losses. These losses occur as follows; theft, losing during transport between floors, counting errors, incomplete billing, order errors. For all these reasons, medication and medical supply management system is needed.

The process of medications within hospital is as follows,

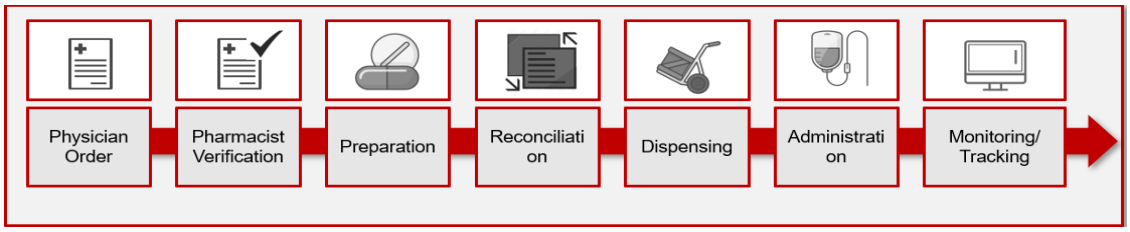

Figure 3. Medication Processes within Hospital

The other process that medical material within hospital is as follows;

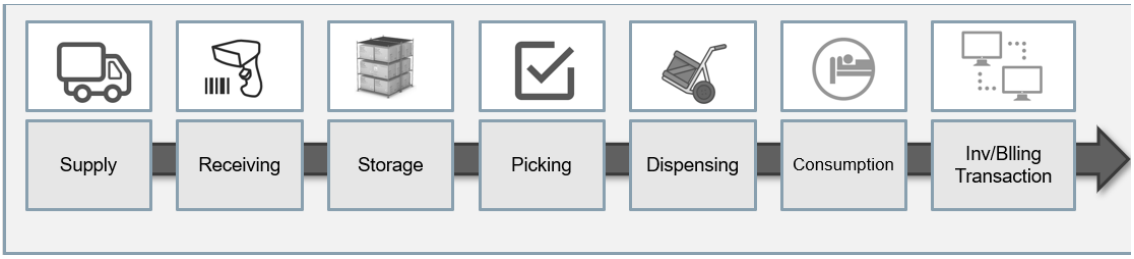

Figure 2. Medical Supply Processes within Hospital

Stocart System is installed every patient unit in hospital and then pharmacy/warehouse load items within Stockart cabinets. In this way, nurses can take directly and easy that their need items. Additionally, every nurse log in system with username and password/bio id/id card combination, in this way, system can follow all of transaction. If medication/medical supply quantity decrease low level, system is alarming pharmacy/warehouse for reloaded. All processes are followed by system and are reported in system database.

System Component

Matrix Drawer

Generally, using for low risk medication management, known as open system.

Sliding Drawer

Generally, using for high risk medication management, known as close system.

Medication Door

Generally, using for high capacity medication management like serum.

Medical Supply Door

Generally, using for medical supply management.

External Module

Generally, using for cold chain medications management.

All of these components compose Stocart System.

2.4.2 Current status and use case challenges

Maintenance process

Stockart System must run 24 hours/ 7 days therefore, components should be always correctly maintained. System maintenance kind is as below;

Planned maintenance

Generally, a planned maintenance is prescribed 1 time per year. The activities performed during the maintenance are defined per configuration. They vary from re-adjusting to proactive cleaning opposite dust. Planned maintenance contain condition

based maintenance activities. Maintenance period can change depending side(hospital) capacity.

Remote Monitoring Engineer (RME)

In nonurgent situations, monitor engineers investigate problem that occur any hardware or software corruption and then try to fix problem via remote control by look in logfile or customer connections.

Field Service Engineer (FSE)

Some hospital installation may be so big and complex, in this case field service engineer need to stay in hospital because FSE must fix every problem within short time due to we cannot predict problem previously.

Remote Service Engineer (RSE)

In new and small installation, FSE doesn't need to stay in hospital. If there is a problem, RSE has to go there for investigation.

Model development

Model to support predictive service will built on top of collected machine data. Typical machine data consists of:

Configuration Data

Identifies the unique composition of the Stockart System, with identifiers for all hardware elements and versions of the hardware

Logfiles

One central logfile across the complete Stockart System contains in an unstructured way the workflow of the system including error events reported by hardware.

Test Data

Test results of tests executed at idle time and test results of tests triggered by FSE and RSE.

The Use Case for Stockart Systems in the context of Daytime is built around the last 3 mentioned challenges, we described our predictive maintenance topics, these are as below;

Solenoid Lock Mechanism Fault

Stockart System has lock mechanism in every component and every lock mechanism has a solenoid motor. Normally solenoid motors are shared lifecycle by manufacturer in this case, we will aim to predict broking time previously thanks to logfile.

Membran Button Bar Fault

Sometimes, membrane button bar which it is used for determining quantity of taken items can broke therefore it cannot run properly. We will aim to predict broking time previously thanks to logfile.

Sliding Drawer Operation Fault

Sliding drawer is used for preserving to high risk medication for this reason always should run under ideal conditions. It has 4 stepper motor, encode, hall effect sensor complex system. Sliding system run with high risk capacity therefore we will aim to predict broking time previously thanks to logfile.

3 State of the art on enabling technologies

3.1 Big data analytics

The term "**Big data**" is often used to describe data sets which are difficult to manage and analyse using standard software tools. This can be due to a considerably large size of the data set and/or its high degree of complexity leading to (unfeasibly) high computational costs. Furthermore, the size which defines a data set as "Big" is an attribute which is time/technology-dependent, e.g., a decade ago data sets of a few Gigabytes were considered challenging to analyse and, thus, classified as "Big data" sets.

Parallel-computing, data-mining, data base optimization/management, and tensor-based computation are some of the concepts which are encompassed by the big data philosophy. Besides that, a considerable number of innovative tools and methods have been recently developed to overcome computational issues associated to big data sets; a few relevant studies reviewed concepts such as: natural language processing, [1,2], machine learning, [3-6], data-mining and information-fusion techniques, [7,8], and others [9-11].

Prognostics and Health Management (PHM) is an emerging discipline focused on understanding and predicting failure mechanisms of safety-critical systems and components as well as managing and optimizing their lifecycle [9,10]. In the PHM context, Big data sets can play a decisive role in predicting the time at which a system will no longer perform as intended. This prediction is often referred to as **Remaining Useful Life** (RUL) and plays a key role in decision making for contingency mitigation. The term Prognostics refers to predictions of the future performance of systems/components. For instance, an extent of deviation, degradation, of a system from its expected normal operating conditions, [12-18]. The term Health Management refers to tools and methods which exploit this prediction to optimize and improve maintenance policies and safety-related decisions, [19-24].

Industrial application of PHM technologies helped solving challenging problems by using the available knowledge, information and data. Examples include, but are not limited to: faults diagnostics and prognostics, [12-14], preventive and corrective maintenance, [15-16], prediction of remaining useful life, [17-18], assets management and part flow management [19-20], maintenance policy optimization and decision-making, [21-24], smart manufacturing, [25].

PHM methods can be divided in 3 main groups [9]:

1) **Data-driven** PHM methods use the available data directly by, e.g., extracting degradation patterns and failure classes. A few examples include, Artificial Intelligence-based approaches (e.g., neural networks, Fuzzy rules, support vector machines, decision trees, and graphical models) and statistical approaches (e.g., principal component method, canonical variates analysis, hypothesis testing, multivariate analysis, signal analysis). Those methods are

particularly useful when the information is abundant, i.e., big data sets, and physical understanding of the failure/degradation mechanisms limited.

2) **Model-based** PHM methods use expert-knowledge and physical knowledge to build high-fidelity physics-based models of the degradation mechanisms, e.g., extended finite elements models, CFD, fatigue models, etc.
3) **Hybrid** PHM methods combine data-driven and model-based approach. For instance, model updating methods estimate a set of parameters of a high-fidelity degradation model (e.g. a set of damages, failure locations and types) which are the most probable explanation for the observed data [12].

References

[1] S. Sun, C. Luo, J. Chen, "A review of natural language processing techniques for opinion mining systems", *Inf. Fusion*, vol. 36, pp. 10-25, 2017.
[2] Y. A. Solangi, Z. A. Solangi, S. Aarain, A. Abro, G. A. Mallah and A. Shah, "Review on Natural Language Processing (NLP) and Its Toolkits for Opinion Mining and Sentiment Analysis," 2018 IEEE 5th International Conference on Engineering Technologies and Applied Sciences (ICETAS), Bangkok, Thailand, 2018, pp. 1-4.
[3] M. Prakash, G. Padmapriy and M. V. Kumar, "A Review on Machine Learning Big Data using R," *2018 Second International Conference on Inventive Communication and Computational Technologies (ICICCT)*, Coimbatore, 2018, pp. 1873-1877.
[4] Yanhui Lin, Xudong Li, Yang Hu, Deep diagnostics and prognostics: An integrated hierarchical learning framework in PHM applications, Applied Soft Computing, Volume 72, 2018, Pages 555-564.
[5] D. Ravì *et al.*, "Deep Learning for Health Informatics," in *IEEE Journal of Biomedical and Health Informatics*, vol. 21, no. 1, pp. 4-21, Jan. 2017.
[6] Thyago P. Carvalho, Fabrízzio A. A. M. N. Soares, Roberto Vita, Roberto da P. Francisco, João P. Basto, Symone G. S. Alcalá, A systematic literature review of machine learning methods applied to predictive maintenance, Computers & Industrial Engineering, Volume 137, 2019.
[7] L. Wang, "Data mining in functional test content optimization," The 20th Asia and South Pacific Design Automation Conference, Chiba, 2015, pp. 308-315.
[8] Alberto Diez-Olivan, Javier Del Ser, Diego Galar, Basilio Sierra, Data fusion and machine learning for industrial prognosis: Trends and perspectives towards Industry 4.0, Information Fusion, Volume 50, 2019, Pages 92-111.
[9] O. E. Dragomir, R. Gouriveau, F. Dragomir, E. Minca and N. Zerhouni, "Review of prognostic problem in condition-based maintenance," 2009 European Control Conference (ECC), Budapest, 2009, pp. 1587-1592.
[10] Bail ey, Chris & Sutharssan, Thamo & Yin, Chunyan & Stoyanov, Stoyan. (2015). Prognostic and health management for engineering systems: a review of the data-driven approach and algorithms. The Journal of Engineering.
[11] Javed, Kamran. (2014). A Robust and Reliable Data-driven Prognostics Approach Based on Extreme Learning Machine and Fuzzy Clustering.
[12] Roberto Rocchetta, Matteo Broggi, Quentin Huchet, Edoardo Patelli, On-line Bayesian model updating for structural health monitoring, Mechanical Systems and Signal Processing, Volume 103, 2018,Pages 174-195.
[13] Piero Baraldi, Francesco Cannarile, Francesco Di Maio, Enrico Zio, Hierarchical k-nearest neighbours classification and binary differential evolution for fault diagnostics of automotive bearings operating under variable conditions, Engineering Applications of Artificial Intelligence, Volume 56, 2016, Pages 1-13.
[14] Baraldi, Piero & Bonfanti, G. & Zio, Enrico. (2018). Differential evolution-based multi-objective optimization for the definition of a health indicator for fault diagnostics and prognostics. Mechanical Systems and Signal Processing. 102. 382-400.

[15] Khanh T.P. Nguyen, Kamal Medjaher, A new dynamic predictive maintenance framework using deep learning for failure prognostics, Reliability Engineering & System Safety, Volume 188, 2019, Pages 251-262.
[16] Pedro Yepez, Basel Alsayyed, Rafiq Ahmad, Intelligent assisted maintenance plan generation for corrective maintenance, Manufacturing Letters, Volume 21, 2019, Pages 7-11.
[17] Cannarile, Francesco & Baraldi, Piero & Zio, Enrico. (2018), An evidential similarity-based regression method for the prediction of equipment remaining useful life in presence of incomplete degradation trajectories. Fuzzy Sets and Systems.
[18] Kaixiang Peng, Ruihua Jiao, Jie Dong, Yanting Pi, A deep belief network based health indicator construction and remaining useful life prediction using improved particle filter, Neurocomputing, Volume 361, 2019, Pages 19-28.
[19] Cannarile, Francesco & Compare, Michele & Di Maio, Francesco & Zio, Enrico. (2018). A Clustering Approach for Mining Reliability Big Data for Asset Management. Proceedings of the Institution of Mechanical Engineers Part O Journal of Risk and Reliability. 232. 10.1177/1748006X17716344.
[20] Compare, Michele & Bellani, Luca & Cobelli, Enrico & Zio, Enrico & Annunziata, Francesco & Carlevaro, Fausto & Sepe, Marzia. (2019). A reinforcement learning approach to optimal part flow management for gas turbine maintenance. Proceedings of the Institution of Mechanical Engineers, Part O: Journal of Risk and Reliability. 1748006X1986975. 10.1177/1748006X19869750.
[21] R. Rocchetta, L. Bellani, M. Compare, E. Zio, E. Patelli, A reinforcement learning framework for optimal operation and maintenance of power grids, Applied Energy, Volume 241, 2019, Pages 291-301.
[22] Pedro Cesar Lopes Gerum, Ayca Altay, Melike Baykal-Gürsoy, Data-driven predictive maintenance scheduling policies for railways, Transportation Research Part C: Emerging Technologies, Volume 107, 2019, Pages 137-154.
[23] Li Yang, Zhi-sheng Ye, Chi-Guhn Lee, Su-fen Yang, Rui Peng, A two-phase preventive maintenance policy considering imperfect repair and postponed replacement, European Journal of Operational Research, Volume 274, Issue 3, 2019, Pages 966-977.
[24] S. Wu, N. Gebraeel, M. A. Lawley and Y. Yih, "A Neural Network Integrated Decision Support System for Condition-Based Optimal Predictive Maintenance Policy," in *IEEE Transactions on Systems, Man, and Cybernetics - Part A: Systems and Humans*, vol. 37, no. 2, pp. 226-236, March 2007.
[25] Ajay Kumar, Ravi Shankar, Lakshman S. Thakur, A big data driven sustainable manufacturing framework for condition-based maintenance prediction, Journal of Computational Science, Volume 27, 2018, Pages 428-439,

3.2 Machine learning

For the medicine cabinet use case, the solenoid lock failures, happen rarely. When a fault happens it is more likely to happen in the future. For these reasons, it is necessary to perform pre and post processing operations on the lock fault data for the medicine cabinet usecase. The preprocessing operations will include the number of faults that happened in a certain time period in the past on a particular cabinet, or on similar (being at the same hospital, being used by the same personnel, having the same repairperson, parts etc.) cabinets. We will also do post-processing on the actual and predicted lock faults to create alarms so that we can reduce the number of false positives.

Features to be used for fault detection: The environmental conditions affect the probability of fault and the humidity data will be provided by the usecase provider.

Although the voltage and current are also important [Zhou2019], for the current usecase, these are controlled through a regulator and will not be included as inputs. The past history of how many times and when the cabinet was opened will also be used as inputs.

In order to reduce complexity of algorithms and to reduce feature selection algorithms will be used. Filter type algorithms that measure feature-label correlation based on mutual information based metrics will be used for feature selection.

Both tree based algorithms and neural networks will be investigated as possible methods. Although the machine learning models will be continuously learning and they will be updated automatically as new data arrive, for the creation of the initial solution we will be using sample data obtained from the usecase provider. The deployment scenarios will be further refined during the project implementation.

Both for the MRI usecase and the Shaver usecase, the pre and post processing, feature selection algorithms will be applied. Similarly, tree and neural network based algorithms and their ensembles [Patil2018] will be used.

References:

[Aleksa2008] Aleksa, M., Bergsma, F., Giudici, P. A., Kehrli, A., Losasso, M., Pons, X., ... & Chevalier, L. (2008). Measurement of the ATLAS solenoid magnetic field. Journal of Instrumentation, 3(04), P04003.

[Guo2018] Guo, W., Cheng, J., Tan, Y., & Liu, Q. (2018, July). Solenoid Valve Fault Diagnosis Based on Genetic Optimization MKSVM. In IOP Conference Series: Earth and Environmental Science (Vol. 170, No. 4, p. 042134). IOP Publishing.

[Murugesan2014] Murugesan, V. M., Chandramohan, G., Kumar, M. S., Rudramoorthy, R., Kumar, L. A., & Palla, R. (2014). Analysis of automobile starter solenoid switch for improved life. automatika, 55(3), 256-264.

[Patil2018] Patil, S., & Phalle, V. (2018). Fault Detection of Anti-friction Bearing using Ensemble Machine Learning Methods. International Journal of Engineering, 31(11), 1972-1981.

[Zhou2019] Zhou, Q., Chen, G., Jiang, W., Li, K., & Li, K. (2019). Automatically Detecting Excavator Anomalies Based on Machine Learning. Symmetry, 11(8), 957.

3.3 Natural language processing

Machines are still often operated and maintained by humans. Everything those humans express, either verbally or written, carries a tremendous amount of information. The topics they choose, their tone, selection of words, everything adds some type of information that can be interpreted and analysed. In theory, we can use such data to make predication about a machine and the humans operating and maintaining it. This also is true for MRI machines maintained by service engineers.

There is however a problem: one service mechanic may generate hundreds or thousands of words in a MRI machine service report, and each sentence comes with its corresponding complexity. If you want to scale and analyse several hundreds or thousands of reports that task becomes unmanageable. This is where a subset of machine learning, namely 'natural language processing' or NLP enters the arena.

Text written by service mechanics is called 'unstructured data'. Unstructured data doesn't fit neatly into the traditional row and column structure of relational databases. With advances in NLP it is possible to convert such unstructured data into structured data, and not just trying to interpret a text based on its keywords, but actually about understanding the meaning behind those words.

Previous research performed by the French aviation industry (Halshs-01322238) showed the potential of NLP to analyse large quantities of textual data in order to find and analyse emerging dangers and risks. A lack of meta data and training data encourages researching unsupervised machine learning techniques such as topic modelling. Standard NLP toolkits use techniques such as 'bag of words', tokenization, stop words removal, stemming and lemmatization. These techniques will be useful to begin with, but more advanced approaches such as open information extraction build algorithms on top of those techniques to extract relationships from text whereby the schema of those relationships does not need to be specified in advance.

Reference

[1] Halshs-01322238: https://halshs.archives-ouvertes.fr/halshs-01322238
[2] https://nlp.stanford.edu/software/openie.html

3.4 Machine log data analysis

Dependent on its purpose, a machine log is a file that typically contains the lead-up to, and outcomes of events originating from machine processes or user inputs. The origin of these logs can be from various devices, applications, operating systems. The contents can vary between formatted text files, or raw data dumps.

While the main use of creating machine logs might have originally been limited to provide insights into the machine's operations or its user inputs, the developments into data analysis have broadened the scope of machine log use cases, such as machine maintenance, system auditability, risk assessment, and concretizing user behaviour [5][2][6].

Moving away from the traditional approach of reactive maintenance, in which equipment is repaired or replaced after break down, the proactive strategy can utilize machine logs to highlight anomalies that are indicative of future issues or to construct a relevant state of the machine, which would allow for performing maintenance actions as soon as the equipment status falls below a pre-determined threshold [15][13].

Depending on the aim of the machine log analysis, there are many methods that can be utilized in performing an analysis. Methods that are commonly used in the overall pipeline are the aggregation, cleaning, structuring and normalization of machine logs. For the aim of machine maintenance, methods are used such as pattern detection and recognition, tagging and classifying key elements in log files, correlation analysis, and anomaly detection [4][17][3].

For a statistical measurement it has been shown that regression is one method that can be used. Ray and Craven [10] employed a comparison study where logistic regression was used in combination with multi-instance learning (MIL) which showed similar results to support vector machines (SVMs). King and Curran [7] used linear regression for predicting semi-conductor failures, while Baptista et al. [2] explored predictive maintenance on aircraft using an auto-regressive moving average algorithm.

Another method is ranking, which was used by Rudin et al. [11] on a series of inspection reports of electrical boxes and manholes and to predict manhole events.

Data analyses based on log files have also been performed through the use of machine learning. Examples of applied supervised learning are the support vector machine (SVM), random forest and ensemble learning, and MIL. Predictive maintenance based on equipment event logs was shown in Sipos et al. [12], where MIL was used in a medical environment. Murray et al. [9] describes how hard drive failure prediction can be accomplished with the use of a SVM, MIL or clustering and found that while computationally expensive the SVM performed best. Research was also performed on the failure estimation for milling machines, where Gutschi et al. [4] used random forest and ensemble predictions. The use of ensemble learning was also used in Zhou and Zhang [18], as an augmentation to existing MIL algorithms, yielding general improvements over the default MIL.

In situations where the target labels are unclear or unknown, there are also unsupervised methods to perform log data analyses, of which examples are clustering and applying a principle component analysis (PCA). Aharon et al. [1] utilized sequential text clustering on system event logs, while Makanju et al. [8] clustered event logs using iterative partitioning. In Devaney et al. [3] log files were clustered first using bootstrapping clustering followed by employing case-based reasoning to identify events leading to machine failures. In addition, Taeret et al. [14] also applied text clustering, while adding heuristics to improve upon handling large data-sets, reduce cluster outliers, and reducing duplicate output patterns. The use of PCAs with performing a log file data analysis was explored in Xu et al. [16], where in the first a PCA was used to extract features indicative of future events, followed by applying decision trees to improve upon explainability. Xu et al. [17] managed to further apply a PCA in an online setting in combination with log files of a Hadoop computational cluster.

References

[1] Aharon, M., Barash, G., Cohen, I., & Mordechai, E. (2009, September). One graph is worth a thousand logs: Uncovering hidden structures in massive system event logs. In Joint European Conference on Machine Learning and Knowledge Discovery in Databases (pp. 227-243). Springer, Berlin, Heidelberg.

[2] Baptista, M., Sankararaman, S., de Medeiros, I. P., Nascimento Jr, C., Prendinger, H., & Henriques, E. M. (2018). Forecasting fault events for predictive maintenance using data-driven techniques and ARMA modeling. Computers & Industrial Engineering, 115, 41-53.

[3] Devaney, M., Ram, A., Qiu, H., & Lee, J. (2005, January). Preventing failures by mining maintenance logs with case-based reasoning. In Proceedings of the 59th meeting of the society for machinery failure prevention technology (MFPT-59).

[4] Gutschi, C., Furian, N., Suschnigg, J., Neubacher, D., & Voessner, S. (2019). Log-based predictive maintenance in discrete parts manufacturing. Procedia CIRP, 79, 528-533.

[5] Huerta, T., Fareed, N., Hefner, J. L., Sieck, C. J., Swoboda, C., Taylor, R., & McAlearney, A. S. (2019). Patient Engagement as Measured by Inpatient Portal Use: Methodology for Log File Analysis. Journal of medical Internet research, 21(3), e10957.
[6] Jansen, B. J., Spink, A., & Taksai, I. (2009). Handbook of research on web log analysis. London: Information Science Reference.
[7] King, R., & Curran, K. (2019). Predictive Maintenance for Vibration-Related failures in the Semi-Conductor Industry. Journal of Computer Engineering & Information Technology,, 8(1), 1.
[8] Makanju, A. A., Zincir-Heywood, A. N., & Milios, E. E. (2009, June). Clustering event logs using iterative partitioning. In Proceedings of the 15th ACM SIGKDD international conference on Knowledge discovery and data mining (pp. 1255-1264). ACM.
[9] Murray, J. F., Hughes, G. F., & Kreutz-Delgado, K. (2005). Machine learning methods for predicting failures in hard drives: A multiple-instance application. Journal of Machine Learning Research, 6(May), 783-816.
[10] Ray, S., & Craven, M. (2005, August). Supervised versus multiple instance learning: An empirical comparison. In Proceedings of the 22nd international conference on Machine learning (pp. 697-704). ACM.
[11] Rudin, C., Passonneau, R. J., Radeva, A., Dutta, H., Ierome, S., & Isaac, D. (2010). A process for predicting manhole events in Manhattan. Machine Learning, 80(1), 1-31
[12] Sipos, R., Fradkin, D., Moerchen, F., & Wang, Z. (2014, August). Log-based predictive maintenance. In Proceedings of the 20th ACM SIGKDD international conference on knowledge discovery and data mining (pp. 1867-1876). ACM.
[13] Swanson, L. (2001). Linking maintenance strategies to performance. International journal of production economics, 70(3), 237-244.
[14] Taerat, N., Brandt, J., Gentile, A., Wong, M., & Leangsuksun, C. (2011). Baler: deterministic, lossless log message clustering tool. Computer Science-Research and Development, 26(3-4), 285.
[15] Tambe, P. P., & Kulkarni, M. S. (2015). A superimposition based approach for maintenance and quality plan optimization with production schedule, availability, repair time and detection time constraints for a single machine. Journal of Manufacturing Systems, 37, 17-32.
[16] Xu, W., Huang, L., Fox, A., Patterson, D. A., & Jordan, M. I. (2008). Mining Console Logs for Large-Scale System Problem Detection. SysML, 8, 4-4.
[17] Xu, W., Huang, L., Fox, A., Patterson, D., & Jordan, M. (2009, December). Online system problem detection by mining patterns of console logs. In 2009 Ninth IEEE International Conference on Data Mining (pp. 588-597). IEEE.
[18] Zhou, Z. H., & Zhang, M. L. (2003, September). Ensembles of multi-instance learners. In European Conference on Machine Learning (pp. 492-502). Springer, Berlin, Heidelberg.

3.5 Predictive analytics for optimizing maintenance activities

Industry 4.0 is named as the fourth industrial revolution which involves concepts like big data, internet of things, the usage of sensors and predictive analytics.
Capital goods are the equipment or machines that are in the primary use of their users on main operations [1]. The example of capital goods can be trains, MRI machines, large scale industry printers. Minimizing maintenance costs and reducing the system downtime for capital goods are important because it affects many parties at once.

Time-based or usage-based maintenance describes the maintenance activity which is planned according to the total usage duration of a part or a system [1]. Maintenance activity is conducted when the usage duration exceeds a pre-determined level. This duration can be measured as usage time in the field (for example if a train is on service

without any maintenance for a certain time period) or the number of times used (for instance number of scans done by an MRI machine) [1].

Condition-based maintenance (CBM) is defined as a decision-making strategy about when to perform the next maintenance action based on a real-time predictive model for a system or components of a system [10]. The actual condition of a part or a system is monitored through either a sensor or periodically during inspections [1]. The aim of the CBM can be predicting the current state of a system, fault detection, identification of abnormalities, which is diagnostic. CBM can be also prognostic when the aim is fault and degradation prediction before faults occur [10]. In general, the diagnostic and prognostic CBM activities are also named as predictive maintenance. The predictive maintenance name is used because predictive analytics are crucial to detect failure when there are signals from the system or determine any failure before happens in the system. The aim of all maintenance activities is minimizing the total cost for the system. This cost may incur in many different forms. Minimizing the system downtime is a primer objective for capital goods. First-Time-Right maintenance is another important goal in order to minimize the costs of maintenance activities.

There exist companies develop predictive analytics solutions to both decreases the total downtime of a system and minimizing the maintenance costs. IBM, SAP, Siemens, Microsoft, and GE are some of the top companies in the market that build solutions for their customer in the area of predictive analytics for maintenance activities [8].

A CBM structure involves sensors and signal-processing techniques to predict the status of a system or component and decision-making models to perform maintenance operations [11]. CBM studies may model degradation level of a component, remaining useful lifetime (RUL), the state of component whether it is failed or not.

There are studies where degradation is modeled by a posterior distribution. Do et al. [4] build a CBM model for parts with stochastic and economic dependencies and use an inspection to collect data and model the degradation model with Gamma distribution. Liu et al. [9] aim to minimize the long-run cost rate, collect data for CBM by inspection and uses Gaussian distribution to model the degradation process. Verbert et al. [17] use Gamma distribution to model the component degradation and builds a decision-making model for maintenance activities based on the degradation model. Elwany and Gabrael [6] build a sensor-driven updating linear and exponential model to determine the RUL of components. Walter and Gero [18] model the component lifetime with Weibull distribution and updates the parameters of distribution with Bayesian update. Zhu and van Houtum [19] use a random coefficient model for the stochastic degradation process in a high setup cost multi-component system.

There are studies which use statistical data-driven approaches to model the degradation process in CBM literature. Rasmekomen and Parlikad [12] use regression to model the degradation of two dependent parts and conduct a sequential CBM optimization model afterward. Cipollini et al. [3] use supervised and unsupervised techniques to determine if a part is decayed or not. They use artificial neural networks (ANNs), Kernel methods, ensemble methods, Bayesian methods, lazy methods and k-nearest neighborhood (kNN) as supervised learning and support vector machines (SVM) as the unsupervised learning algorithm. They use a threshold policy for the probability of a part being decayed to conduct the maintenance activity or not. Susto et al. [13] use SVM and kNN to build a multiple classifier for predictive maintenance model on a high dimensional, unbalanced and censored data. Hu et al. [7] use the ensemble data-driven prognostic approach

which combines multiple-member algorithms with a weighted sum formulation. Tian et al. [15] compute life percentage of a component by using ANN in order to determine the health condition. Tian [15] uses ANN for RUL estimation.

In order to make novel models in CBM area, it is important to determine the gaps in the literature. Peng et al. [10] have an extensive literature review on condition-based maintenance. After their survey, they point out two possible extensions in the field: (1) There is a need for more models that combines prognostic models and decision making together. (2) There is a need for more generalized models, which will be not specific to a machine or component type.

Bertsimas and Kallus [2] point out that there is an opportunity of using multi-dimensional predictive models (data mining and machine learning models) in optimal decision making. The maintenance area now has more real-time data than ever. There is an opportunity for building more sophisticated estimations using machine learning and data mining approaches and implementing the results of these models into the optimal decision-making models. Tulabandhula and Rudin [14] have studies on machine learning with operational costs. The main approach involves embedding the error function of the prediction model into the objective function with operational costs. As pointed out by these studies, there is a gap in maintenance literature for the studies combining adaptive decision-making models with learning for both single and multi-dimensional data. There are techniques used in different fields rather than maintenance [2,14] which handles similar problems. It is crucial to develop similar models in the maintenance domain since there are enough data available with the developing sensor technologies and improving storage of data.

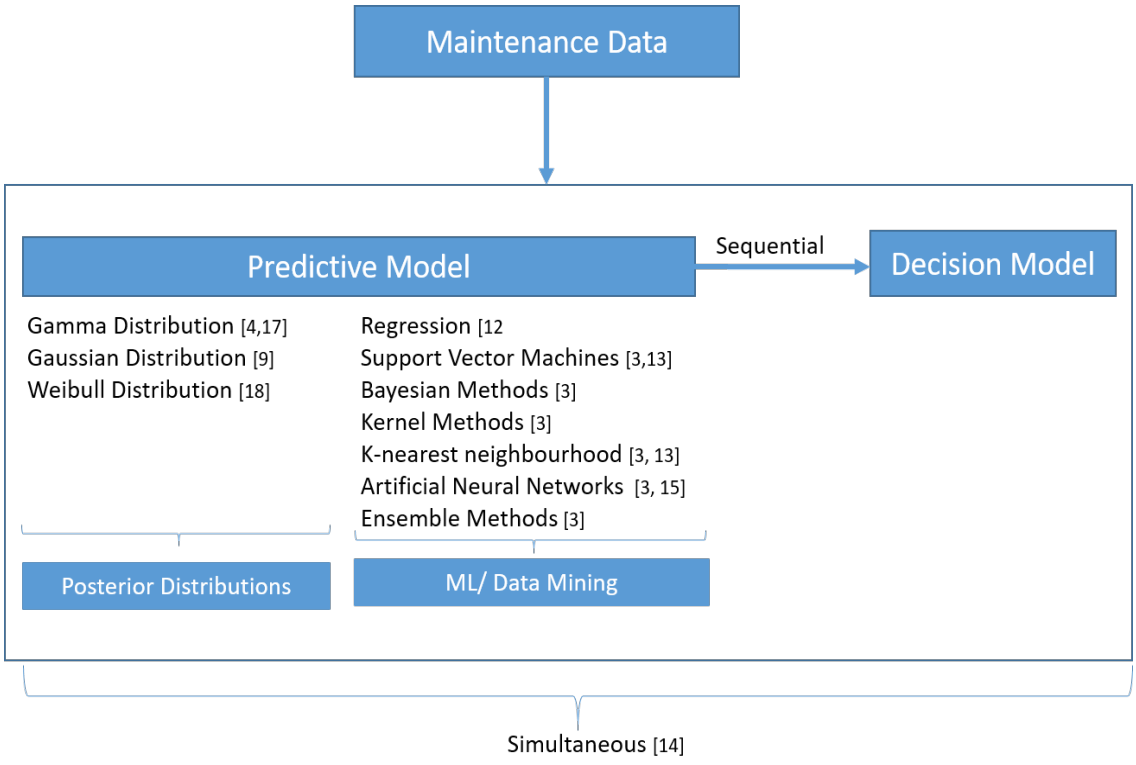

Figure: Summary of structure of CBM models in state-of-art analysis

References

[1] Arts J., Basten R., van Houtum GJ. (2019) Maintenance Service Logistics. In: Zijm H., Klumpp M., Regattieri A., Heragu S. (eds) Operations, Logistics and Supply Chain Management. Lecture Notes in Logistics. Springer, Cham

[2] Bertsimas, D., & Kallus, N. (2014). From predictive to prescriptive analytics. arXiv preprint arXiv:1402.5481.

[3] Cipollini, F., Oneto, L., Coraddu, A., Murphy, A. J., & Anguita, D. (2018). Condition-based maintenance of naval propulsion systems: Data analysis with minimal feedback. *Reliability Engineering & System Safety*, *177*, 12-23.

[4] Do, P., Assaf, R., Scarf, P., Iung, B. (2019) Modelling and application of condition-based maintenance for a two-component system with stochastic and economic dependencies, Reliability Engineering & System Safety, Volume 182, Pages 86-97, ISSN 0951-8320, https://doi.org/10.1016/j.ress.2018.10.007.

[5] Do, P., Voisin, A., Levrat, E., & Iung, B. (2015). A proactive condition-based maintenance strategy with both perfect and imperfect maintenance actions. Reliability Engineering & System Safety, 133, 22-32.

[6] Elwany, A. H., & Gebraeel, N. Z. (2008). Sensor-driven prognostic models for equipment replacement and spare parts inventory. IIE Transactions, 40(7), 629-639.

[7] Hu, C., Youn, B. D., Wang, P., & Yoon, J. T. (2012). Ensemble of data-driven prognostic algorithms for robust prediction of remaining useful life. *Reliability Engineering & System Safety*, *103*, 120-135.

[8] Iot-analytics.com, (2017), Top 20 companies enabling predictive maintenance. Retrieved by https://iot-analytics.com/top-20-companies-enabling-predictive-maintenance/, on 20 August 2019.

[9] Liu, B., Liang, Z., Parlikad, A. K., Xie, M., & Kuo, W. (2017). Condition-based maintenance for systems with aging and cumulative damage based on proportional hazards model. *Reliability Engineering & System Safety*, *168*, 200-209.

[10] Peng, Y., Dong, M., & Zuo, M. J. (2010). Current status of machine prognostics in condition-based maintenance: a review. The International Journal of Advanced Manufacturing Technology, 50(1-4), 297-313.

[11] Raheja, D.,Llinas, J., Nagi, R., & Romanowski, C. (2006) Data fusion/data mining-based architecture for condition-based maintenance, International Journal of Production Research, 44:14, 2869-2887, DOI: 10.1080/00207540600654509

[12] Rasmekomen, N., & Parlikad, A. K. (2016). Condition-based maintenance of multi-component systems with degradation state-rate interactions. *Reliability Engineering & System Safety*, *148*, 1-10.

[13] Susto, G. A., Schirru, A., Pampuri, S., McLoone, S., & Beghi, A. (2014). Machine learning for predictive maintenance: A multiple classifier approach. *IEEE Transactions on Industrial Informatics*, *11*(3), 812-820.

[14] Tulabandhula, T., & Rudin, C. (2013). Machine learning with operational costs. The Journal of Machine Learning Research, 14(1), 1989-2028.

[15] Tian, Z. (2012). An artificial neural network method for remaining useful life prediction of equipment subject to condition monitoring. *Journal of Intelligent Manufacturing*, *23*(2), 227-237.

[16] Tian, Z., Jin, T., Wu, B., & Ding, F. (2011). Condition based maintenance optimization for wind power generation systems under continuous monitoring. *Renewable Energy*, *36*(5), 1502-1509.

[17] Verbert, K., De Schutter, B., & Babuška, R. (2017). Timely condition-based maintenance planning for multi-component systems. *Reliability Engineering & System Safety*, *159*, 310-321.

[18] Walter, G. M., & Flapper, S. D. P. (2017). Condition-based maintenance for complex systems based on current component status and Bayesian updating of component reliability. Reliability Engineering and System Safety, 168, 227-239. DOI: 10.1016/j.ress.2017.06.015

[19] Zhu, Q., Peng, H., & Houtum, van, G. J. J. A. N. (2012). A condition-based maintenance policy for multi-component systems with a high maintenance setup cost. (BETA publicatie : working papers; Vol. 400). Eindhoven: Technische Universiteit Eindhoven.

3.6 Sensor technology

Introduction

The growing demand for flexible, ultrasensitive wearable sensors for myoelectric prosthesis, soft robotics, and personalized health monitoring applications has been the main driving factor behind the rapid advancement in soft and flexible material processing technologies. In particular, human motion monitoring devices are emerging to be the most sought-after wearable devices as they can potentially provide a host of valuable information regarding the health and well-being of an individual [1].

Traditionally, piezoelectric, piezoresistive and capacitive transduction mechanisms have mostly been exploited in the development of flexible sensors to convert strain stimuli into electrical signals. Inorganic piezoelectric materials such as lead zirconate titanate (PZT), zinc oxide (ZnO), barium titanate ($BaTiO_3$) [2–7] and soft piezoelectric polymers like polyvinylidene fluoride (PVDF) and polyvinylidene fluoride-trifluoroethylene (PVDF-TrFE) [8–12] have been explored extensively for developing various flexible sensors in the past. On the other hand, though piezoresistive microelectromechanical systems (MEMS) sensors using metallic and semiconductor-based strain gauges have been quite popular for strain sensing applications owing to the well-established fabrication processes and large measurement range, their application as wearable sensors is limited due to their high stiffness and low stretchability [13,14]. Flexible and squeezable sensors utilizing the piezoresistive property of nanomaterial-elastomer composites are relatively new, and researchers across the globe have been exploring various combinations of novel nanomaterial and suitable elastomer for developing a new generation of innovative, flexible piezoresistive sensors [15–21]. Polymer materials like polydimethylsiloxane (PDMS), ecoflex, polyimide (PI), rubber and polyurethane (PU) have been commonly used as the flexible polymer substrates due to their superior flexibility compressibility, and excellent responsiveness to torsion, tension, and compression [16,18,22–24]. To make the sensors low–cost, renewable and biodegradable, a recent work reported having used printing paper substrate as a novel alternative to traditional elastomers [25]. For the conductive nanomaterials, silver nanowires (AgNWs) and various types of carbon-based materials like carbon nanotubes (CNTs), carbon nanofibers (CNFs), carbon blacks (CBs), and graphene have been explored by researchers [18,19,26–32]. Of all the conductive carbon-based nanomaterials, recently, graphene has been exploited the most for developing nanomaterial-polymer composite-based piezoresistive sensors mainly because of its excellent conductivity, stiffness, and elastic properties [16,22,33]. The most common method of developing graphene based piezoresistive sensors has been the use of nanoporous graphene foams synthesized by chemical vapour deposition (CVD) process. Due to the fragility of freestanding 3-D graphene foams, they are infiltrated with elastomers like PDMS to enhance their mechanical properties like elasticity and durability. Pang et al. proposed a novel method involving infiltration of PDMS in graphene-coated nickel foam template and subsequent etching to preserve graphene nanoporous structure with PDMS scaffold for developing a highly sensitive piezoresistive sensor [16]. Recently, researchers have

also reported graphene-based fiber sensors for various strain monitoring applications [31,34]. A recently published review article presents a detailed overview of the developments in the field of flexible polymer-based strain sensors and discusses the recent developments in the field of electrically conductive polymer composites [35].

Most of the Graphene-elastomer foam/spongy materials reported so far either employed fragile free-standing foamy graphene structure or involved sophisticated multistep fabrication methods involving polymer infiltration in graphene coated template and subsequent etching. In addition, most of these works focused on the synthesis of the spongy nanomaterials; however, their applications as sensing materials to develop 3D squeezable sensors was not investigated [36–38]. In this work, we proposed a facile process of developing an ultralightweight and highly squeezable 3D microporous graphene-PDMS foam-based sensor. Sugar cubes were used as templates for developing microporous PDMS foams, followed by dip coating of the foams in conductive multilayered graphene (MLG) suspension to infiltrate them with graphene nanoflakes. The porous graphene-infiltrated foams were studied employing a scanning electron microscope (SEM) to understand its strain-induced resistance modulation mechanism and conductive domain disconnection mechanism was invoked to explain its piezoresistive property. The density of the graphene-PDMS foam sensors was calculated to be 0.305 g cm^{-3} owing to the porous structure. The response of the graphene-PDMS sensors developed with the proposed method was characterized for static and dynamic pressure stimuli. From the static and dynamic compressive strain tests, the response of the sensor was found to have two linear regions with average gauge factor lying in the range 2.87 ~ 8.77. Accelerated lifetime tests were conducted on the spongy sensor through cyclic compressive loading involving 36000 load cycles to demonstrate its overall reliability and durability. The responses of the sensors to dynamic loading were characterized to observe their sensing performance at high frequency strain loading. Finally, the application of these sensors in monitoring both simulated and real-time human gait and other body motion parameters was validated through experiments which demonstrate the broad applicability of such sensors in various applications including personalized health monitoring, soft robotics, myoelectric prosthesis and other wearable devices. Three identical sensors were assembled on a soft shoe-sole and used in synchronization to differentiate between the pressure profiles under a low arch/flat foot and a medium arch foot. The sensor assembly was also used for demonstrating the capability for real-time gait characteristics acquisition and differentiation between different kinds of human movements, including walking, running, periodic leaning, and standing. The simple method of sensor development demonstrated in this work will guide the development of a future generation of 3D squeezable and highly sensitive pressure/strain sensors suitable for various high-performance wearable, and flexible devices.

3D Squeezable graphene-PDMS foam sensor

Sensor fabrication and morphological study: The process steps involved in fabrication of the graphene-PDMS squeezable strain sensor are schematically illustrated in **Figure 1**a. The experimental details of the fabrication process are described in the materials and methods section. The electrical connections for acquiring electrical outputs from the

sensor were made by smearing and subsequently curing a thin layer of conductive silver epoxy on the two sides of the graphene-PDMS foam as shown in **Figure 1**b. The optical images shown in **Figure 1**c and d, demonstrate the compressibility and ultra-light weight of the developed sensor respectively. Furthermore, the squeezability of the sensor was demonstrated by holding it between two fingers and applying a series of squeeze-release cycles (shown in the attached supplementary video file).

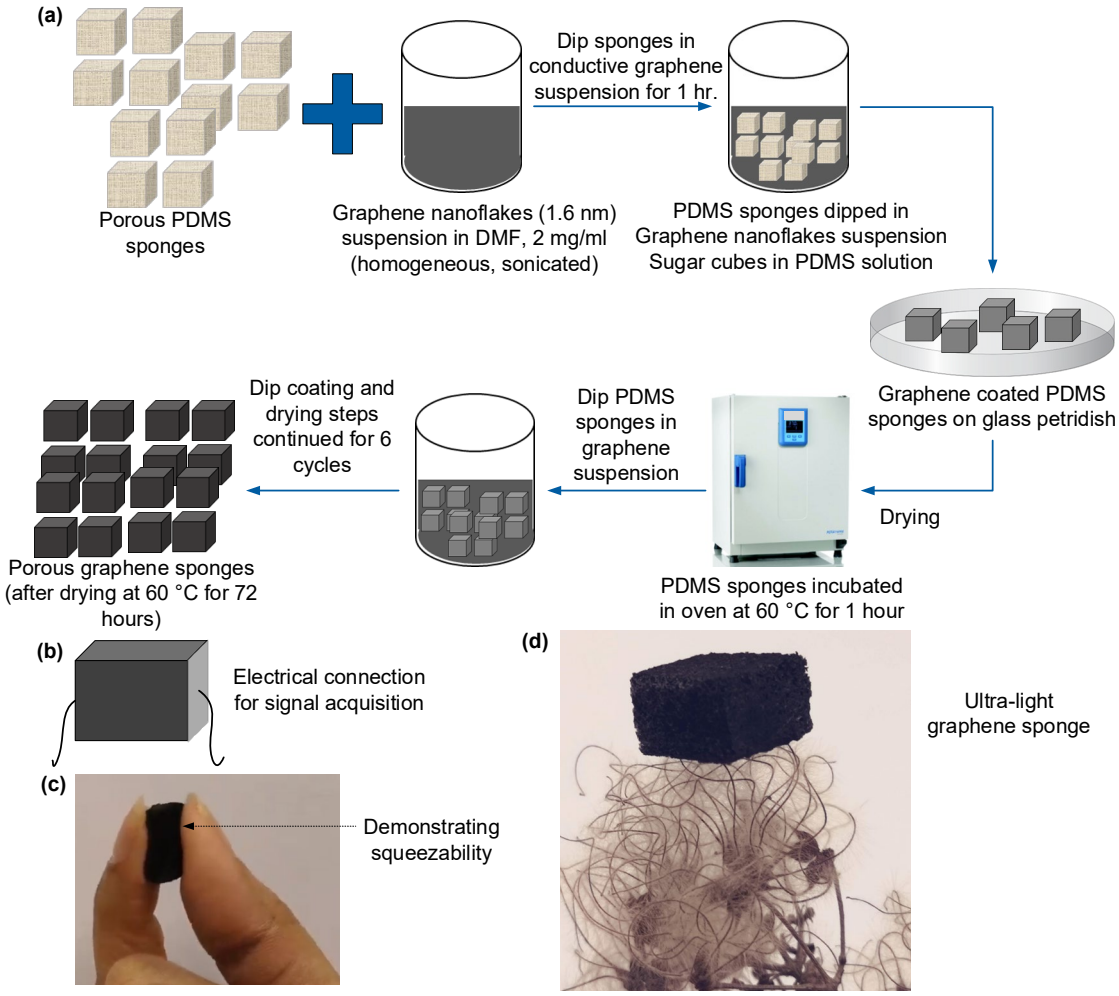

Figure 1. Fabrication of the squeezable graphene-PDMS foam sensor: (a) Schematic representation of infiltrating PDMS foam with multilayered graphene nanoflakes (MLG); (b) schematic representation of a single PDMS-MLG foam sensor with electrical contacts; (c) the squeezability and (d) ultra-light nature of the graphene-PDMS foam sensor.

Multiple dip coating and drying cycles of the PDMS sponge in homogeneous graphene / N,N-dimethyl formamide (DMF) suspension led to the attachment of multilayered graphene nano-flakes (MLG) in the inner pore walls of the micro-porous PDMS substrate. **Figure 2**a and b show the SEM micrographs of the unloaded PDMS foam. An average pore diameter of 386 µm was observed for the developed PDMS foam (averaged over eight measurements on different sponges). **Figure 2**c and d show the SEM micrographs after loading the PDMS with MLG. As the SEM

micrographs clearly depict, the graphene nanoflakes penetrated into the porous structure of the PDMS foam and attached themselves onto the inner walls of the micro-porous structure.

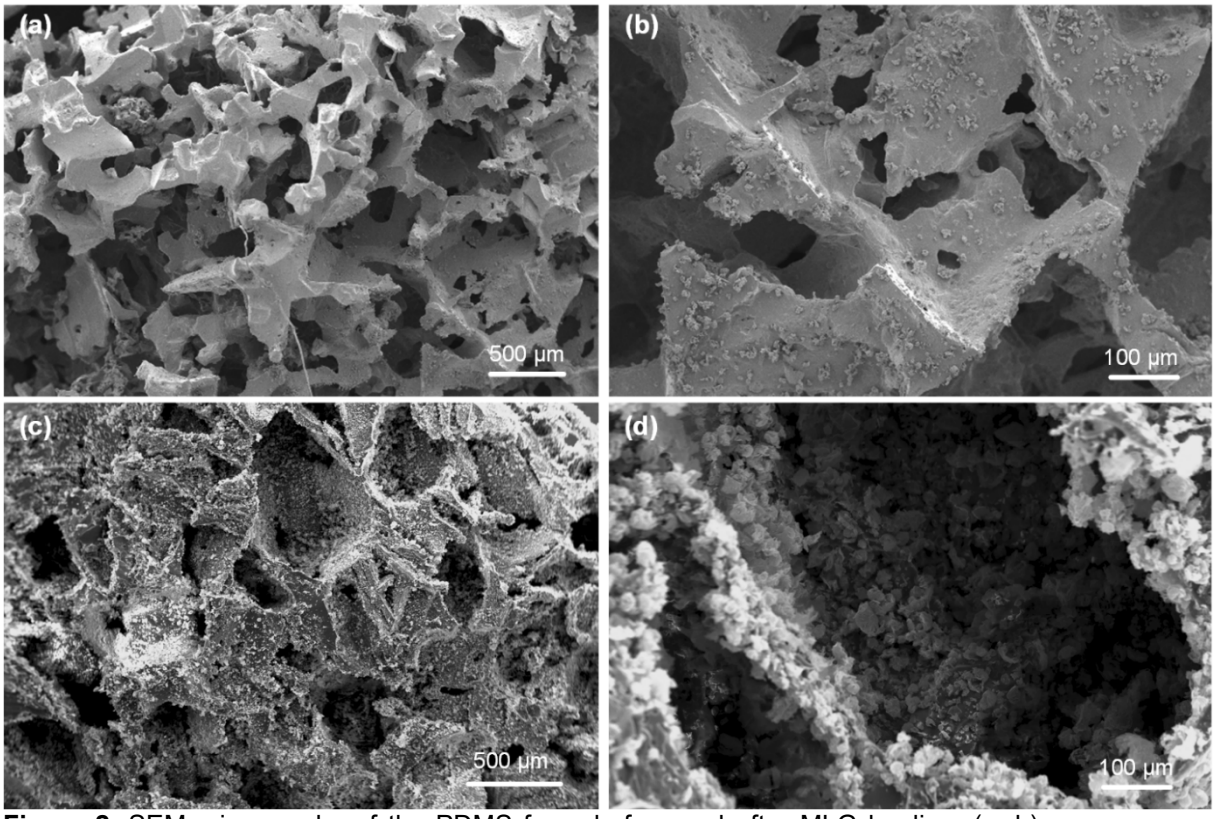

Figure 2. SEM micrographs of the PDMS foam before and after MLG loading: (a, b) porous structure of the unloaded PDMS foam at different magnifications; (c, d) MLG loaded PDMS foam at two different magnifications with the pore walls covered with MLG nanoflakes forming a nanomaterial percolation network.

The strain-responsive resistance change mechanism in the graphene-PDMS foam could arise from the conductive domain disconnection mechanism which was also reported in the past for other types of thin films made of nanomaterials [19,24,39–41]. Within the MLG nanomaterial flake network, electrons pass through the overlapping network of conductive MLG flakes. Application of external force/stress causes a change in the overlapping area between the conductive MLG flakes thus leading to a change in resistance as schematically explained in **Figure 3**a. Also, electrons can tunnel across a thin polymer barrier separating two adjacent nanomaterial domains thus forming quantum tunneling junctions. The tunneling resistance between two adjacent graphene nanoflakes separated by a polymer layer can be predicted using Simmon's tunneling resistance theory [42]. In the past, researchers have reported a tunneling cutoff distance of 2-3 nm between two parallel graphene sheets separated by polymer insulation [43,44]. Upon application of pressure, a pore wall may get compressed enough so that the effective distance between two graphene nanoflakes adhering to the opposite sides of the wall may reduce to 2nm or less in which case electrons will be able to tunnel across the PDMS wall barrier. **Figure 3**b schematically explains the stress-induced tunneling resistance modulation. Given the relatively large size of the pores, it can be safely

assumed that the strain-responsive piezoresistivity in the graphene-PDMS foams reported in this paper originates mostly due to the conductive domain disconnection mechanism (while the stress-induced tunneling resistance modulation mechanism plays a minimal to no role at all), wherein an external force/stress causes the graphene nanoflakes to slide against each other thus leading to a large change in overall resistance of the graphene-PDMS foam sensor.

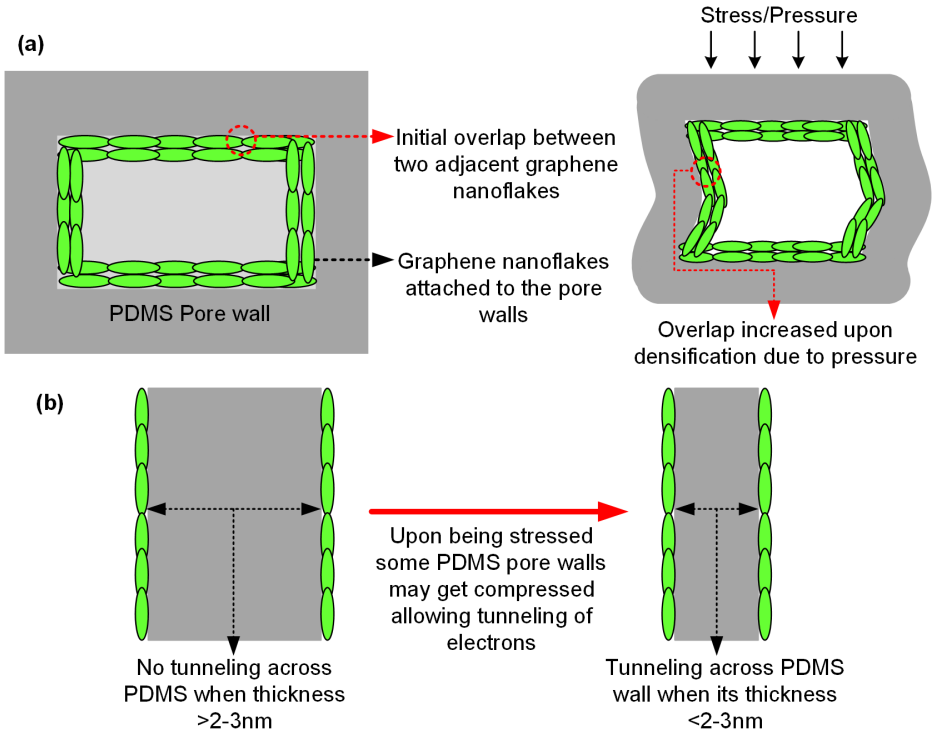

Figure 3. Schematic diagram explaining the possible strain induced resistance modulation mechanisms in graphene-PDMS foam sensor: (a) Schematic explaining the conductive domain disconnection mechanism explaining strain induced resistance modulation observed in the sensor; (b) Schematic representation of stress-induced tunneling resistance modulation.

Strain sensor characterization: The Graphene-PDMS foam sensors were characterized under various strain loading conditions including static and dynamic loading in order to demonstrate its applications for flexible and wearable sensors. **Figure 4**a shows the schematic representation of the experimental setup used for the characterization of the sensors (details provided in materials and methods section). An initial pre-compression of 1% was applied to avoid problems related to initial sliding/settling of graphene nanoflakes, which are observed in similar types of squeezable sensors developed in the past [33]. A compressive strain was applied in steps of 0.5% all the way up to 9.5%. After attaining a peak compressive strain of 9.5%, the strain was released in steps of 0.5% to return to the starting position. The experiment was repeated three times, and no noticeable delay was observed between the piston extension and the sensor response throughout the duration of the experiment. With increasing compressive strain, the resistance of the sensor was observed to decrease linearly for strains up to 9.5%. **Figure 4**b shows the plot of the modulus of normalized resistance change calculated from the data acquired from the Wheatstone bridge circuit versus the compressive strain. The

output of the sensor was observed to increase linearly with increasing strain for compressive strains up to 9.5 %. The data was treated with a linear regression fit to estimate the compressive gauge factor ($G.F. = \frac{\Delta R}{R} / \frac{\Delta L}{L}$) of the graphene-PDMS foam. The compressive gauge factor of the sensor was determined to be 8.77 from the slope of the linear regression. To assess the strain sensing performance of the graphene-PDMS foam sensor for larger strains, the sensor was subjected to five different maximum compressive cyclic strains (10%, 20%, 30%, 40%, and 50%) at a constant frequency of 5 Hz using a mini-shaker setup as depicted in the schematic in **Figure 4**c (details of the experimental setup are provided in the materials and methods section). The minishaker was driven with a square-wave stimulus at a constant frequency of 5 Hz, which resulted in cyclic compressive stains in the sponge. The sensor outputs were recorded for at least 50 cycles at each of the aforementioned maximum strain levels, and the normalized resistance changes were calculated and plotted for the individual compressive strain cycles as shown in **Figure 4**d. **Figure 4**e shows the superimposed plots of the normalized resistance change demonstrated by the sensor in response to the five maximum compressive strain cycles (appropriate band-pass filter was used to eliminate the 50 Hz power supply interference). The data from the cyclic compressive strain characterization experiment were analyzed, and the mean normalized resistance change values were determined individually for each of the five different maximum compressive strain levels. Furthermore, the gauge factor of the sponge was determined individually for each of the aforementioned compressive strain values and plotted in the form of a bar graph, as shown in **Figure 4**f. From the plots in **Figure 4**b and f, two distinct regions of operations (of the graphene-PDMS foam sensor) can be identified. The sensor demonstrated a reasonably linear response for strain levels up to 9.5%. A sharp decrease in the gauge factor was observed for strains exceeding 10%. The decrease in the gauge factor at higher strain rates can be attributed to the fact that at higher strain values, the inter-nanoparticle distances are continuously bridged and hence, the sensor reaches near network saturation [45]. Thus, saturation in the percentage decrease in resistance for higher compressive strain levels is observed, which is clearly reflected by the reduced gauge factor values (at higher strain levels exceeding 10%). Similar response characteristics have been observed for similar nanoparticle-elastomer composite foam-based sensors in the past [16,45]. **Table 1** compares the gauge factor of our graphene-PDMS foam sensor with some other sensors reported by various researchers in the past.

Table 1**.** Summarizing the gauge factors of various flexible strain sensors reported in the past.

Material	Gauge factor	Linearity
AgNWs-PDMS [19]	2 ~ 14	Linear up to 40%
CNTs-Ecoflex [18]	1 ~ 2.5	Linear
Aligned SWCNTs-PDMS [26]	0.82	Two linear regions
Carbon Black-PDMS [27]	1.8 ~ 5.5	Two linear regions
Carbon Black-Ecoflex [46]	3.8	Nonlinear

Single CNF strain sensor [47]	1.96 ~ 2.55	Linear
GPN-PDMS [16]	2.6 ~ 8.5	Two linear regions
Graphene-Rubber [24]	35	Linear and exponential regions
Graphene ink-on-PDMS [48]	37	Linear
Graphene-PDMS foam (This work)	2.87 ~ 8.77	Two linear regions

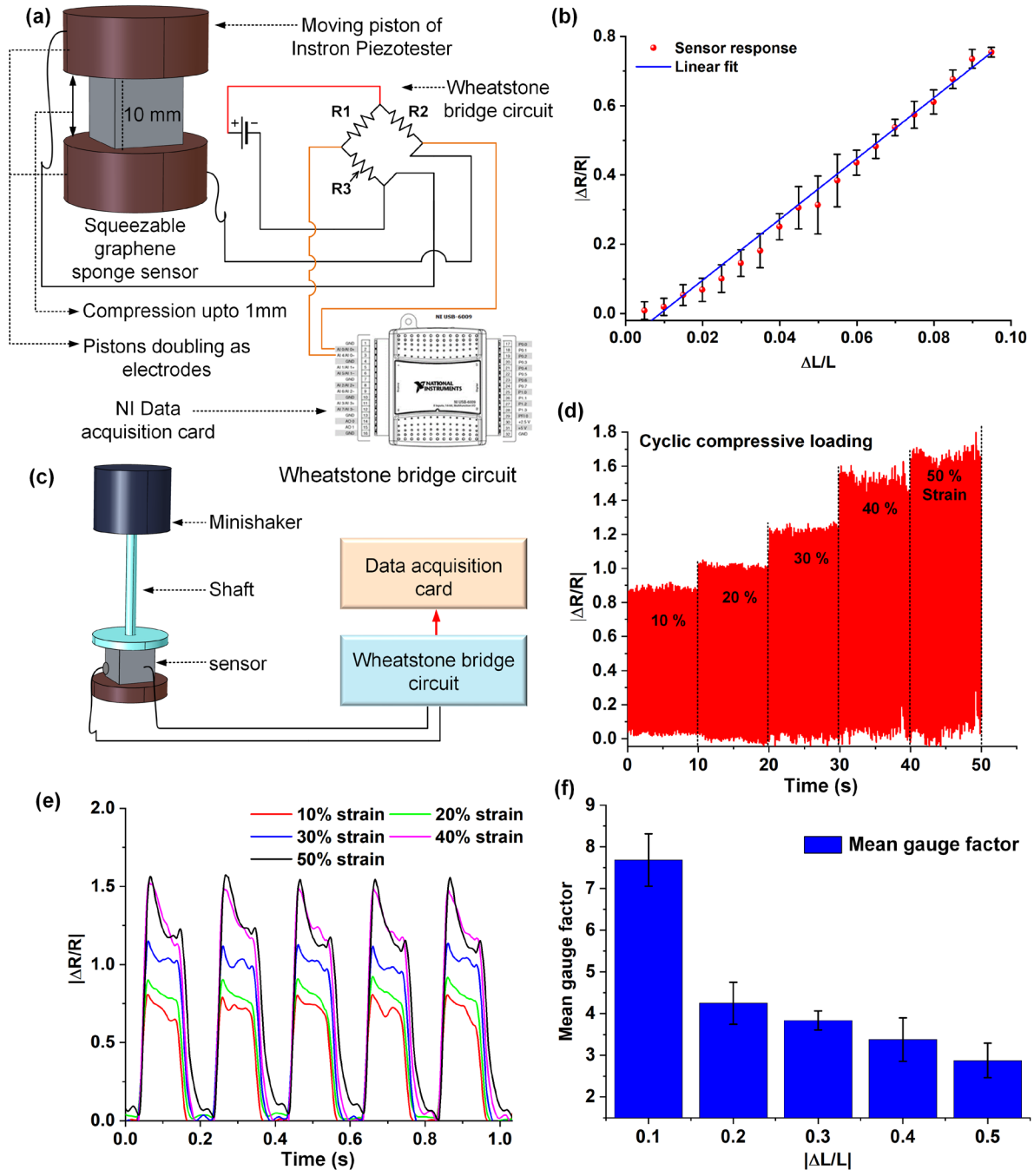

Figure 4. Graphene-PDMS foam sensor characterization: (a) Schematic representation of the setup used for conducting the piezoresistivity characterization experiments; (b) Plot of normalized resistance change in the graphene-PDMS foam sensor versus

applied compressive strain up to 9.5%; (c) Schematic representation of the setup used for conducting the piezoresistivity characterization experiments for larger compressive strains in the range ~ 10-50%; (d) Plot showing the sensor response in terms of normalized resistance change when subjected to five different compressive loading at different strains (between 10% to 50%); (e) Superimposition plot showing the normalized resistance change of the sensor for five different compressive strains between 10% and 50%; (f) Bar chart showing the calculated gauge factor for the graphene-PDMS foam sensor for the five different compressive strains between 10% and 50%.

Reliability test and dynamic response characterization: To demonstrate the long-time reliability of the graphene-PDMS foam sensor, an accelerated life testing was conducted on the sensor by subjecting it to a series of 36000 cyclic compressive loading and unloading at 5% compressive strain using the same experimental setup previously shown in **Figure4**c. The minishaker was driven at a constant frequency of 10 Hz and the power amplifier driving the setup was set such that the compressive strain generated was approximately 5%. The sensor response was acquired from the Wheatstone bridge circuit, and an appropriate band-pass filter was applied to eliminate the 50 Hz power supply interference. **Figure 5**a shows the normalized resistance change plots acquired from the reliability tests. A zoomed-in plot placed on the right-hand side of the main plot shows the consistency of the sensor response cycles for the applied cyclic compressive strains.

To further evaluate the strain sensing performance of the sensor under dynamic loading conditions, the graphene-PDMS foam sensor was subjected to compressive strains at three different frequencies using the same mini-shaker setup described previously. The minishaker was driven with square-wave stimuli at three different frequencies (10 Hz, 35 Hz, and 70 Hz), which caused compression of the sponge at those frequencies. **Figure 5**b shows the as-acquired sensor response for the oscillatory test conducted at 10 Hz. For the 35 Hz and 70 Hz stimuli, the sensor responses were acquired and treated with appropriate low-pass filters in order to eliminate the 50 Hz power supply interference. Fast Fourier transform (FFT) was carried out on the individual responses to determine the average amplitude of the sensor response as shown in **Figure 5**c. The sensor amplitude responses were observed to have increased with applied stimulus frequency.

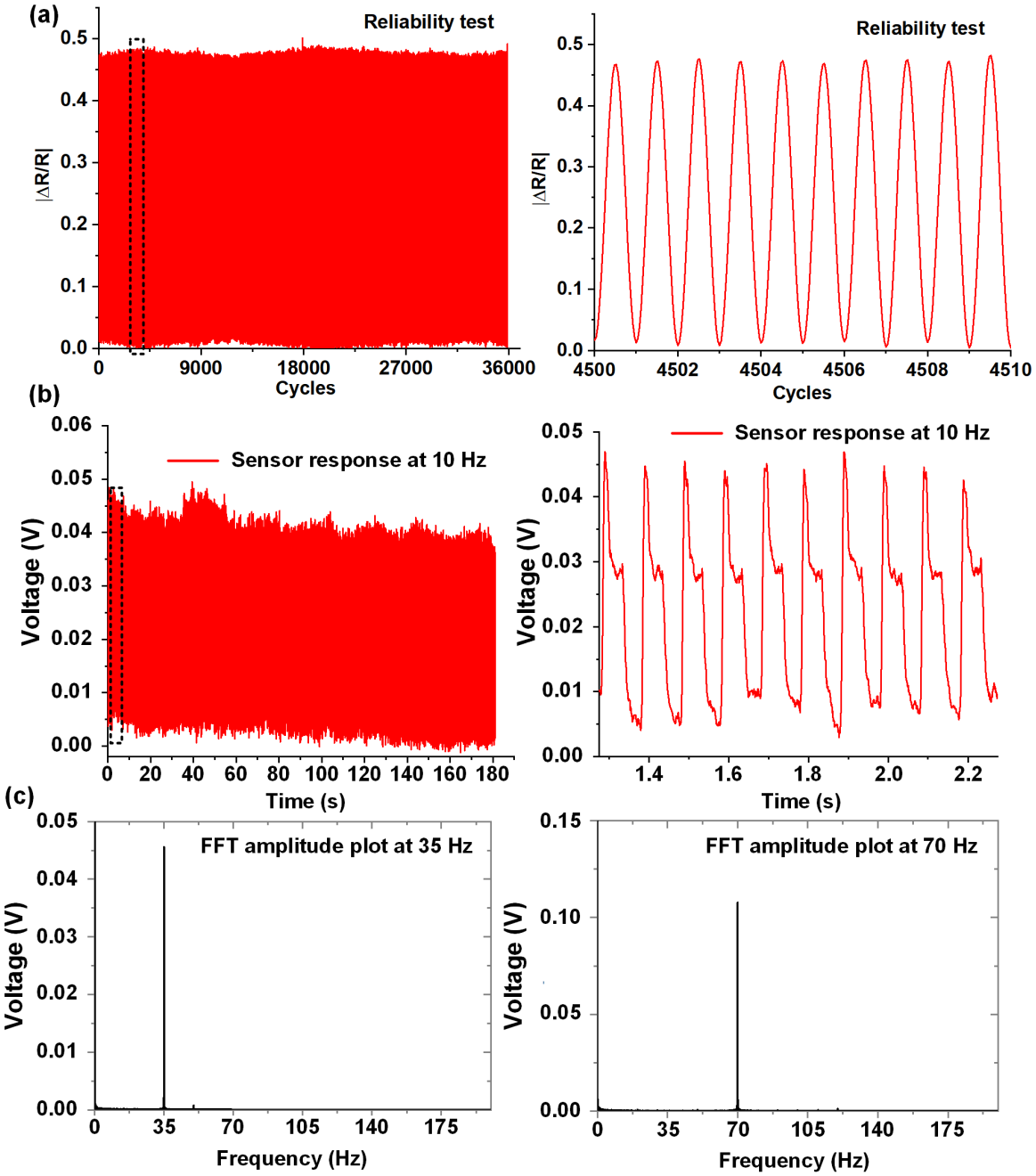

Figure 5. Cyclic compressive loading and dynamic strain sensing characterization of the graphene-PDMS foam sensor: (a) Response of the sensor to cyclic loading and unloading at 5% compressive strain. The figure on the right shows the zoomed-in version of the plot; (b) Plot showing the sensor response at 10 Hz in time domain; Zoomed in plot on the right showing the sensor response at 10 Hz in the interval 1.3-2.3 seconds; (c) FFT amplitude plot showing the sensor responses at 35 Hz and 70 Hz respectively.

Sensor applications

Application of the graphene-PDMS foam for human motion monitoring: Continuous monitoring of gait characteristics can enable early diagnosis of diseases like strokes, multiple sclerosis, and Parkinson's disease thus enabling personalized treatment plans

for patients [1]. To demonstrate the applicability of the graphene-PDMS foam sensors in gait monitoring, a gait simulation response experiment was conducted using the Instron 5940 UTS™ (details of the experimental setup are provided in the materials and methods section). The pressure behavior under the heel of a walking person was appropriately mimicked employing simulated gait models applied to the movable piston of the test system. The pressure pattern under the heel of a walking individual comprises of a gradual ramping up to the maximum pressure (body weight divided by the area of the heel pad), followed by a partial pressure release and finally ramping down to a complete pressure release when the heel is lifted off the ground [49]. Due to limitations of the test setup used, the force ramp up and ramp down rate was slow (20 mm/min movement of piston) due to which each gait cycle lasted 30 seconds unlike in real human being where each gait cycle lasts 1.08 ± 0.11 seconds [50]. The experiment was carried out for 45 gait cycle repetitions to demonstrate the consistency in sensor response. **Figure 6**a shows the sensor response for the gait simulation experiment. The zoomed-in version of **Figure 6**a (right) shows the sensor response for four complete gait cycles. The schematics diagrams in the figure inset explain the sensor response by comparing it to the heel movement. Overall, a good consistency was observed in the sensor response throughout the gait simulation experiment.

To demonstrate the capability of the sensor for real-time gait and foot pressure monitoring, three identical graphene-PDMS sensors were attached and secured on a soft flat shoe-sole with the intention of acquiring the sensor response from three distinct pressure points (toe ball, foot arch, and heel) of the right foot as shown in **Figure 6**b. The shoe sole-sensor assembly (SSA) was placed inside a shoe and worn by a person with a medium arch foot. **Figure 6**c shows the response of the sensor (acquired real-time) while the person walked slowly. For this work, the sensor responses from the toe ball and the heel regions are shown as these are the two most intense pressure regions in the medium arch biomechanically efficient foot. The phase lag between sensors from the toe ball and heel region demonstrates the walking behavior of the person. While walking, when the heel is placed down, the pressure increases to a maximum value followed by subsequent relaxation while the whole foot is placed down on the floor. At the point where the foot is completely down on the floor, the two sensor response curves intersect each other indicating equal pressure distribution. As the heel is lifted slowly while placing the toe ball down on the floor, the pressure of the toe ball increases up to a maximum, and the pressure of the heel decreases to a minimum value. This behavior is repeated throughout the entire duration of walking, as shown by the sensor response plot in **Figure 6**c. The SSA was also applied for real-time running pressure variation monitoring. As shown by the plot in **Figure 6**d, the pressure response is very different from walking. In the case of running or jogging, most of the impact is absorbed by the toe ball followed by the middle arch, which is reflected clearly by the sensor response plot. Furthermore, the phase lag characteristics differ significantly from normal walking. To demonstrate the capability of the SSA in detecting pressure variation, the person wearing it leaned forward and backward in a periodic fashion leading to a periodic pressure distribution variation between the toe ball and the heel. As expected, the sensor response plot in **Figure 6**e clearly shows the phase lag between the toe ball and heel sensor pressure response. Interestingly, the pressure variation from the foot arch

(middle sensor) is relatively less compared to the other two regions which can be attributed to the fact that the maximum share of weight of a human body is borne by the toe ball and heel which leads to larger pressure concentration in those two regions in comparison to the foot arch region.

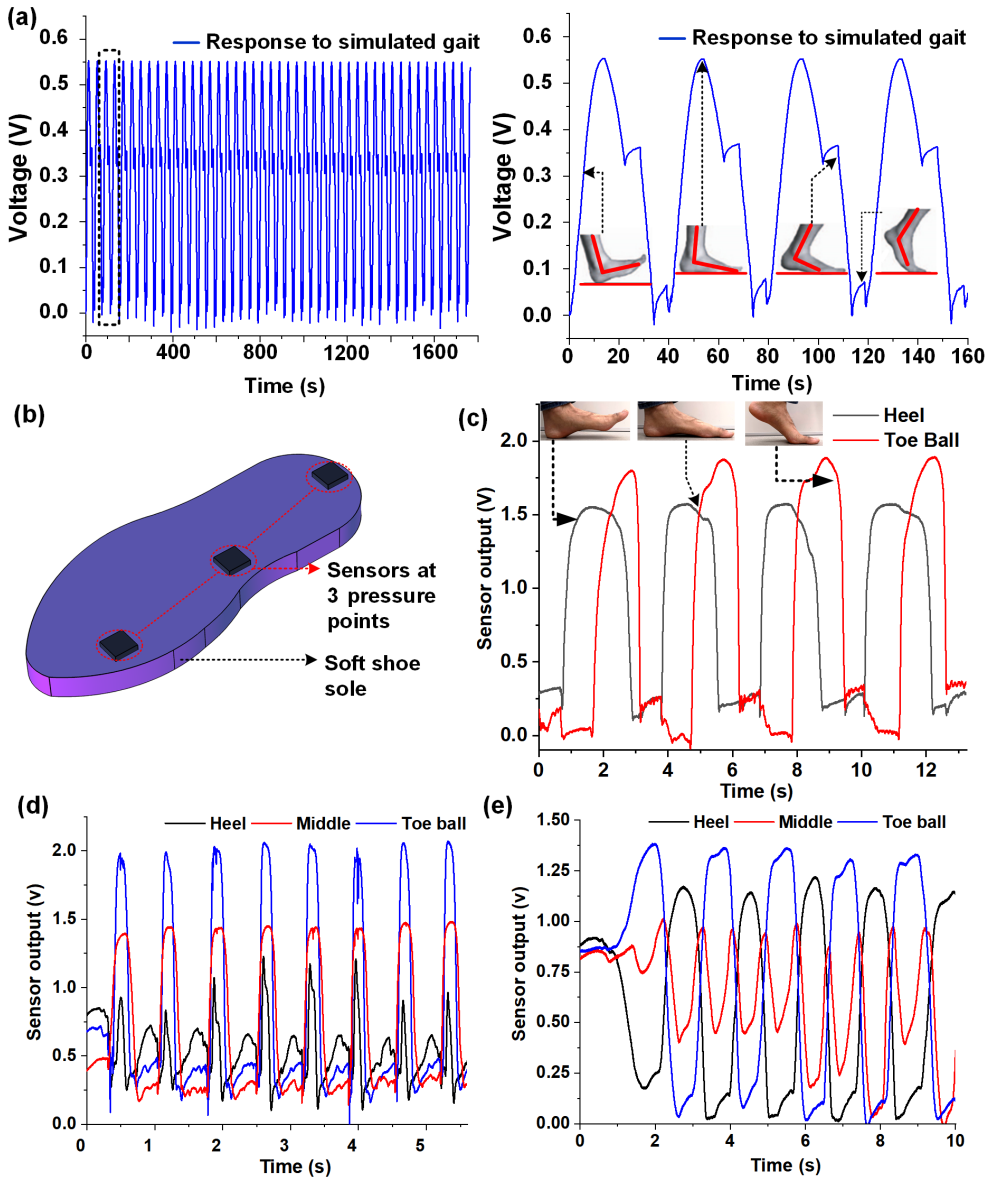

Figure 6. Application of the graphene-PDMS foam sensor for human gait monitoring: (a) Response plot of the sensor to simulated gait; Plot on the right shows zoomed in version of the sensor response over four gait cycles with schematics explaining heel positioning; (b) Schematic representation of the soft shoe sole sensor assembly (SSA); (c) Plot showing the sensor responses from the toe ball and heel regions while walking; (d) Plot showing the sensor responses from the toe ball, foot arch and heel regions while running; (e) Plot showing sensor responses from the toe ball, foot arch and heel regions while leaning forward and backward in a periodic fashion.

The fact that the maximum share of the weight of a human body is borne by the toe ball and heel (which leads to larger pressure concentration in those two regions in

comparison to the foot arch region) was utilized to differentiate between a low arch (flat) foot and a medium arch foot using the SSA. **Figure 7**a compares a low arch/flat foot with a medium arch foot. Due to the difference in the anatomies of the two feet types, their pressure profiles are distinct and different. As seen in the figure, low arch-type foot typically has a foot arch sitting low to the ground and hence it has significantly more pressure concentration in the middle foot arch region in comparison to the medium arch foot. To demonstrate the capability of the SSA in distinguishing between the two different foot types, the setup was worn by a person with a flat foot, and the pressure response was recorded while the foot was placed down. The experiment was repeated on a person with a medium arch foot. The plots in **Figure 7**b show the SSA responses acquired from the persons with the two different foot types. As expected, the SSA response from the person with low arch/flat foot indicates a more even pressure distribution between the three pressure regions. Whereas, the SSA response acquired from the person with medium arch foot shows a more skewed pressure distribution with the toe ball and heel sharing the maximum share of the load in comparison to the middle arch region. The experiments demonstrate the capability of the SSA to distinguish between the different feet anatomies.

Furthermore, to demonstrate the applicability of the sensor in sensing finger and wrist joint movement, the senor was secured on a wearable nitrile glove which was then worn to demonstrate working on the sensor. Five cycles of finger and wrist flicking were carried out and the output from the balanced Wheatstone bridge circuit to which the sensor was connected was recorded as shown in **Figure 7**c and d. The experiments conducted demonstrate the feasibility of using such sensors for developing wearable biomedical devices for health monitoring applications.

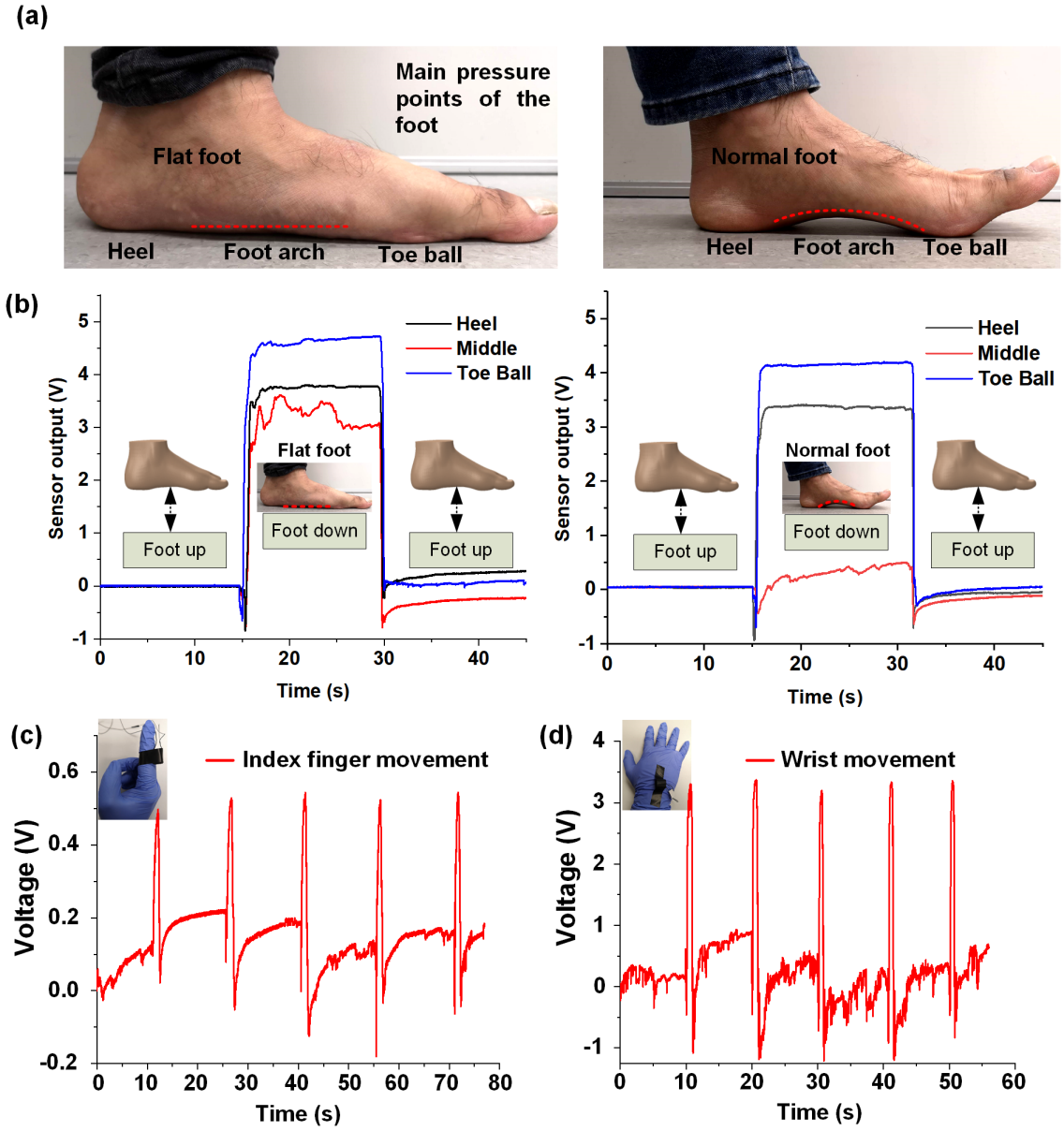

Figure 7. Application of the graphene-PDMS foam sensor for distinguishing between foot anatomies and human motion monitoring: (a) Images comparing a low arch/flat foot with a medium arch biomechanically efficient foot; (b) Plot comparing the SSA pressure responses acquired from the two different foot types. The pressure distribution in case of the low arch foot is more even compared to the medium arch foot; (c) Response of the sensor to index finger flick; (d) Response of the sensor to wrist flick.

Conclusions

In conclusion, this work presented a facile method for developing graphene-PDMS foam-based ultralightweight (having a density of 0.31 g cm^{-3}), squeezable, linear, and highly sensitive sensor. The sensor demonstrated in this work utilized a microporous PDMS substrate with graphene nanoflakes attached to its inner pore walls forming an MLG percolation network which responds to pressure/strain by virtue of the conductive domain disconnection mechanism. To support the theory of conductive domain

disconnection mechanism (which explains the strain-responsive resistance change property demonstrated by the sensor), SEM microscopic studies were conducted, which revealed the attachments of graphene nanoflakes on the inner pore walls of the PDMS foam substrate thus backing up our hypothesis. The sensor was subjected to a series of static and dynamic strain stimuli response tests to evaluate its sensing performance and repeatability. The sensor responses were found to be linear, and the average gauge factor was determined to be 8.77 for compressive strains up to 10%. For compressive strains exceeding 10%, the gauge factor was found to vary between 2.87 ~ 8.77 (in the strain range of 10 ~ 50%). To demonstrate the feasibility of applying the sensor for various wearable devices and personalized health monitoring applications, both simulated and real-time gait responses and other human monitoring experiments were conducted. A soft shoe-sole sensor assembly was fabricated and demonstrated to identify various gait characteristics, including walking, running, periodic leaning, and standing. The sensor assembly was also found to be capable of differentiating the foot types based on their middle arch architecture. The simple method for developing highly sensitive, lightweight and squeezable piezoresistive sensors demonstrated in this work will inspire a future generation of inexpensive and highly efficient pressure and strain sensors suitable for human motion detection and personalized health monitoring applications.

References

(1) Wall, J. C.; Turnbull, G. I. Gait Asymmetries in Residual Hemiplegia. *Arch. Phys. Med. Rehabil.* **1986**, *67* (8), 550–553.

(2) Aktakka, E. E.; Peterson, R. L.; Najafi, K. A CMOS-Compatible Piezoelectric Vibration Energy Scavenger Based on the Integration of Bulk PZT Films on Silicon. In *Technical Digest - International Electron Devices Meeting, IEDM*; 2010, 31- 35.

(3) Wang, X. Y.; Lee, C. Y.; Peng, C. J.; Chen, P. Y.; Chang, P. Z. A Micrometer Scale and Low Temperature PZT Thick Film MEMS Process Utilizing an Aerosol Deposition Method. *Sensors Actuators, A Phys.* **2008**, *143* (2), 469–474.

(4) Chen, X.; Xu, S.; Yao, N.; Shi, Y. 1.6 V Nanogenerator for Mechanical Energy Harvesting Using PZT Nanofibers. *Nano Lett.* **2010**, *10* (6), 2133–2137.

(5) Wang, Z. L.; Song, J. Piezoelectric Nanogenerators Based on Zinc Oxide Nanowire Arrays. *Science* **2006**, *312* (5771), 242–246.

(6) Qin, Y.; Qin, Y.; Wang, X.; Wang, X.; Wang, Z. L.; Wang, Z. L. Microfibre-Nanowire Hybrid Structure for Energy Scavenging. *Nature* **2008**, *451* (7180), 809–813.

(7) Wang, X.; Song, J.; Liu, J.; Wang, Z. L. Direct-Current Nanogenerator Driven by Ultrasonic Waves. *Science* **2007**, *316* (5821), 102–105

(8) Sengupta, D.; Kottapalli, A. G. P.; Chen, S. H.; Miao, J. M.; Kwok, C. Y.; Triantafyllou, M. S.; Warkiani, M. E.; Asadnia, M. Characterization of Single Polyvinylidene Fluoride (PVDF) Nanofiber for Flow Sensing Applications. *AIP Adv.* **2017**, *7* (10), 105205.

(9) Liu, Z. H.; Pan, C. T.; Lin, L. W.; Huang, J. C.; Ou, Z. Y. Direct-Write PVDF Nonwoven Fiber Fabric Energy Harvesters via the Hollow Cylindrical near-Field Electrospinning Process. *Smart Mater. Struct.* **2014**, *23* (2).

(10) Sencadas, V.; Moreira, M. V.; Lanceros-Méndez, S.; Pouzada, A. S.; Gregório

Filho, R. α- to β Transformation on PVDF Films Obtained by Uniaxial Stretch. *Mater. Sci. Forum* **2006**, *514–516*, 872–876.

(11) Dargaville, T. R. T.; Celina, M. C.; Elliot, J.; Chaplya, P. M.; Elliott, J. M.; Jones, G. D.; Mowery, D. M.; Assink, R. a; Clough, R. L.; Martin, J. W. Characterization, Performance and Optimization of PVDF as a Piezoelectric Film for Advanced Space Mirror Concepts. *Optimization* **2005**, SAND2005-6846.

(12) Wang, Y. R.; Zheng, J. M.; Ren, G. Y.; Zhang, P. H.; Xu, C. A Flexible Piezoelectric Force Sensor Based on PVDF Fabrics. *Smart Mater. Struct.* **2011**, *20* (4), 045009.

(13) Cao, L.; Kim, T. S.; Mantell, S. C.; Polla, D. L. Simulation and Fabrication of Piezoresistive Membrane Type MEMS Strain Sensors. *Sensors Actuators, A Phys.* **2000,** *80* (3), 273-279.

(14) Da Silva, J. G.; De Carvalho, A. A.; Da Silva, D. D. A Strain Gauge Tactile Sensor for Finger-Mounted Applications. *IEEE Trans. Instrum. Meas.* **2002**, *51* (1), 18-22.

(15) Alamusi; Hu, N.; Fukunaga, H.; Atobe, S.; Liu, Y.; Li, J. Piezoresistive Strain Sensors Made from Carbon Nanotubes Based Polymer Nanocomposites. *Sensors*. **2011**, *11* (11), 10691-10723.

(16) Pang, Y.; Tian, H.; Tao, L.; Li, Y.; Wang, X.; Deng, N.; Yang, Y.; Ren, T. Flexible, Highly Sensitive, and Wearable Pressure and Strain Sensors with Graphene Porous Network Structure. *ACS Appl. Mater. Interfaces* **2016**, *8* (40), 26458–26462.

(17) Zhao, J.; He, C.; Yang, R.; Shi, Z.; Cheng, M.; Yang, W.; Xie, G.; Wang, D.; Shi, D.; Zhang, G. Ultra-Sensitive Strain Sensors Based on Piezoresistive Nanographene Films. *Appl. Phys. Lett.* **2012**, *101* (6), 063112.

(18) Amjadi, M.; Yoon, Y. J.; Park, I. Ultra-Stretchable and Skin-Mountable Strain Sensors Using Carbon Nanotubes-Ecoflex Nanocomposites. *Nanotechnology* **2015**, *26* (37), 375501.

(19) Amjadi, M.; Pichitpajongkit, A.; Lee, S.; Ryu, S.; Park, I.; Engineering, M.; Sensor, M.; Convergence, I. T.; Korea, S. Highly Stretchable and Sensitive Strain Sensor Based on Silver Nanowire À Elastomer Nanocomposite. **2014**, No. 5, 5154–5163.

(20) Thuau, D.; Ayela, C.; Poulin, P.; Dufour, I. Highly Piezoresistive Hybrid MEMS Sensors. *Sensors Actuators, A Phys.* **2014**, 209, 161-168.

(21) Wisitsoraat, A.; Patthanasetakul, V.; Lomas, T.; Tuantranont, A. Low Cost Thin Film Based Piezoresistive MEMS Tactile Sensor. *Sensors Actuators, A Phys.* **2007**, *139* (1-2), 17-22.

(22) Qin, Y.; Peng, Q.; Ding, Y.; Lin, Z.; Wang, C.; Li, Y.; Xu, F.; Li, J. Mechanically Flexible Graphene / Polyimide Nanocomposite Foam for Strain Sensor Application. **2015**, No. 9, 8933–8941.

(23) Yao, H.; Ge, J.; Wang, C.; Wang, X.; Hu, W.; Zheng, Z. COMMUNICATION A Flexible and Highly Pressure-Sensitive Graphene – Polyurethane Sponge Based on Fractured Microstructure Design. **2013**, *25* (46), 6692–6698.

(24) Boland, C. S.; Khan, U.; Backes, C.; O'Neill, A.; McCauley, J.; Duane, S.; Shanker, R.; Liu, Y.; Jurewicz, I.; Dalton, A. B.; et al. Sensitive, High-Strain, High-Rate Bodily Motion Sensors Based on Graphene-Rubber Composites. *ACS Nano* **2014,** *8* (9), 8819-8830.

(25) Li, Q.; Liu, H.; Zhang, S.; Zhang, D.; Liu, X.; He, Y.; Mi, L.; Zhang, J.; Liu, C.; Shen, C.; et al. Superhydrophobic Electrically Conductive Paper for Ultrasensitive Strain

Sensor with Excellent Anticorrosion and Self-Cleaning Property. *ACS Appl. Mater. Interfaces* **2019**, *11* (24), 21904-21914.

(26) Yamada, T.; Hayamizu, Y.; Yamamoto, Y.; Yomogida, Y.; Izadi-Najafabadi, A.; Futaba, D. N.; Hata, K. A Stretchable Carbon Nanotube Strain Sensor for Human-Motion Detection. *Nat. Nanotechnol.* **2011**, *6* (5), 296.

(27) Kong, J.-H.; Jang, N.-S.; Kim, S.-H.; Kim, J.-M. Simple and Rapid Micropatterning of Conductive Carbon Composites and Its Application to Elastic Strain Sensors. *Carbon N. Y.* **2014**, *77*, 199–207.

(28) Sengupta, D.; Kottapalli, A. G. P.; Chen, S. H.; Michael, A.; Kwok, C. Y.; Miao, J.; Triantafyllou, M. S. Flexible Graphitized Polyacrylonitrile Nanofiber Bundles for Strain Sensors. In *NEMS 2018 - 13th Annual IEEE International Conference on Nano/Micro Engineered and Molecular Systems*; **2018**.

(29) Liu, H.; Dong, M.; Huang, W.; Gao, J.; Dai, K.; Guo, J.; Zheng, G.; Liu, C.; Shen, C.; Guo, Z. Lightweight Conductive Graphene/Thermoplastic Polyurethane Foams with Ultrahigh Compressibility for Piezoresistive Sensing. *J. Mater. Chem. C* **2017**, *5* (1), 73–83.

(30) Zhang, S.; Liu, H.; Yang, S.; Shi, X.; Zhang, D.; Shan, C.; Mi, L.; Liu, C.; Shen, C.; Guo, Z. Ultrasensitive and Highly Compressible Piezoresistive Sensor Based on Polyurethane Sponge Coated with a Cracked Cellulose Nanofibril/Silver Nanowire Layer. *ACS Appl. Mater. Interfaces* **2019**, *11* (11), 10922–10932.

(31) Huang, T.; He, P.; Wang, R.; Yang, S.; Sun, J.; Xie, X.; Ding, G. Porous Fibers Composed of Polymer Nanoball Decorated Graphene for Wearable and Highly Sensitive Strain Sensors. *Adv. Funct. Mater.* **2019**,1903732.

(32) Liu, Q.; Chen, J.; Li, Y.; Shi, G. High-Performance Strain Sensors with Fish-Scale-Like Graphene-Sensing Layers for Full-Range Detection of Human Motions. *ACS Nano* **2016**, *10*(8), 7901-7906.

(33) Rinaldi, A.; Tamburrano, A.; Fortunato, M.; Sarto, M. S. A Flexible and Highly Sensitive Pressure Sensor Graphene Nanoplatelets. *Sensors* **2016**, *16* (12), 2148.

(34) Cheng, Y.; Wang, R.; Sun, J.; Gao, L. A Stretchable and Highly Sensitive Graphene-Based Fiber for Sensing Tensile Strain, Bending, and Torsion. *Adv. Mater.* **2015**. https://doi.org/10.1002/adma.201503558.

(35) Liu, H.; Li, Q.; Zhang, S.; Yin, R.; Liu, X.; He, Y.; Dai, K.; Shan, C.; Guo, J.; Liu, C.; et al. Electrically Conductive Polymer Composites for Smart Flexible Strain Sensors: A Critical Review. *Journal of Materials Chemistry C*. **2018**, *6* (45), 12121-12141.

(36) Tran, D. N. H.; Losic, D. Selective Adsorption of Oil–Water Mixtures Using Polydimethylsiloxane (PDMS)–Graphene Sponges. *Env. Sci: Water Research and tecnology* **2015**, *1* (3), 298-305.

(37) Nguyen, D. D.; Tai, N. H.; Lee, S. B.; Kuo, W. S. Superhydrophobic and Superoleophilic Properties of Graphene-Based Sponges Fabricated Using a Facile Dip Coating Method. *Energy Environ. Sci.* **2012**, *5* (7), 7908-7912.

(38) Liu, Y.; Ma, J.; Wu, T.; Wang, X.; Huang, G.; Liu, Y.; Qiu, H.; Li, Y.; Wang, W.; Gao, J. Cost-Effective Reduced Graphene Oxide-Coated Polyurethane Sponge as a Highly Efficient and Reusable Oil-Absorbent. *ACS Appl. Mater. Interfaces* **2013**, *5* (20), 10018-10026.

(39) Xiao, X.; Yuan, L.; Zhong, J.; Ding, T.; Liu, Y.; Cai, Z.; Rong, Y.; Han, H.; Zhou, J.;

Wang, Z. L. High-Strain Sensors Based on ZnO Nanowire / Polystyrene Hybridized Flexible Films. *Adv. Mat.* **2011**, *23* (45), 5440–5444.
(40) Hempel, M.; Nezich, D.; Kong, J.; Hofmann, M. A Novel Class of Strain Gauges Based on Layered Percolative Films of 2D Materials. *Nano Letters* **2012**, *12* (11), 5714-5718.
(41) Park, J. J.; Hyun, W. J.; Mun, S. C.; Park, Y. T.; Park, O. O. Highly Stretchable and Wearable Graphene Strain Sensors with Controllable Sensitivity for Human Motion Monitoring. *ACS Appl. Mater. Interfaces* **2015**. *7* (11), 6317-6324.
(42) Amjadi, M.; Kyung, K.; Park, I.; Sitti, M. Stretchable , Skin-Mountable , and Wearable Strain Sensors and Their Potential Applications : A Review. *Adv. Funct. Mater.* **2016**, *26* (11), 1678–1698.
(43) Oskouyi, A. B.; Sundararaj, U.; Mertiny, P. A Numerical Model to Study the Effect of Temperature on Electrical Conductivity of Polymer-CNT Nanocomposites; 2014.
(44) Hicks, J.; Behnam, A.; Ural, A. A Computational Study of Tunneling-Percolation Electrical Transport in Graphene-Based Nanocomposites. *Appl. Phys. Lett.* **2009**, *95* (21), 213103.
(45) Charara, M.; Luo, W.; Saha, M. C.; Liu, Y. Investigation of Lightweight and Flexible Carbon Nanofiber/Poly Dimethylsiloxane Nanocomposite Sponge for Piezoresistive Sensor Application. *Adv. Eng. Mater.* **2019**, *21* (5), 1801068.
(46) Muth, J. T.; Vogt, D. M.; Truby, R. L.; Mengüç, Y.; Kolesky, D. B.; Wood, R. J.; Lewis, J. A. Embedded 3D Printing of Strain Sensors within Highly Stretchable Elastomers. *Adv. Mater.* **2014,** *26* (36), 6307-6312.
(47) Cai, J.; Chawla, S.; Naraghi, M. Piezoresistive Effect of Individual Electrospun Carbon Nanofibers for Strain Sensing. *Carbon* **2014**, *77*, 738–746.
(48) Kamat, A. M.; Pei, Y.; Kottapalli, A. G. P. Bioinspired Cilia Sensors with Graphene Sensing Elements Fabricated Using 3D Printing and Casting. *Nanomaterials* **2019**, *9* (7), 954.
(49) Chi, K. J.; Schmitt, D. Mechanical Energy and Effective Foot Mass during Impact Loading of Walking and Running. *J. Biomech.* **2005**, *38* (7), 1387–1395.
(50) Murray, M. P.; Kory, R. C.; Clarkson, B. H. Walking Patterns in Healthy Old Men. *J. Gerontol.* **1969,** *24* (2), 169-178.

3.7 Visualization and simulation

Data visualization can be performed in many ways and on many different platforms. Visualization types range from graphs and scatter plots, to hand-made drawings (e.g. architectural drawings) and finally fully interactive 3D rendered scenes. In the context of Daytime, we will manly focus on interactive 3D visualizations.

Traditionally, visualizations are created on large workstations and take many hours to render a single static scene. This type of visualization is still common practice in the areas of movie and video production, where animated movies are rendered in huge render farms. This process results in photo-realistic images, at the cost of high rendering times. With these kinds of rendering times, creating interactive 3D visualizations is impossible. Therefore, different rendering techniques have to be used in order to enable interactive 3D visualization.

For photo-realistic rendering, ray-tracing is the most common rendering technique. With this technique, physical lighting is simulated by simulating rays of light being cast by light sources and reflecting off all objects in the scene. In order to get a high-quality rendered image, a large number of rays (often millions of them) are used to generate an image. Computing these rays is a very costly process and the cause of the long rendering times. Other techniques include path-tracing, photon mapping and radiosity. Each of them requires a large amount of computations to simulate the physical behavior of light and is therefore costly to use.

Real-time rendering is mostly polygon-based and done by rasterization engines. In this case, each object in the scene is constructed from multiple primitives (polygons) that are one-by-one transformed to pixels on the screen by a rasterizer. Different processing steps are then performed on the polygons and the final image to make the final image look more realistic. This procedure is significantly faster compared to ray-tracing and offers rendering speeds enabling high frame-rates.

Recent developments in the area of GPUs have opened up the possibility to perform ray-tracking in real time on certain types of state-of-the art Nvidia GPUs. This opens up new possibilities for photorealistic rendering in interactive 3D visualization settings, but currently requires specific hard- and software to be used. In the near future, real-time ray-tracing will become available more widely.

Another aspect of visualization is the platform on which the images are viewed. Specifically, for real-time interactive 3D visualization, different platforms are available offering a completely different user experience.

Traditional display of 3D visualizations is done on PC monitors and movie screens. These show a 2D representation of the rendered 3D scene. The introduction of 3D displays and stereo glasses made it possible to visualize 3D scenes in stereoscopic 3D, making the visualizations more immersive and natural. These techniques can be used for interactive as well as non-interactive visualizations.

The current state-of-the-art in visualization is the use of virtual reality (VR) and augmented reality (AR) goggles, also called head mounted displays (HMDs). HMDs enable a user to be fully immersed in the visualized scene by offering a stereo image together with head tracking interaction. Because of this, they require a certain level of interaction in order to be used. Using these kinds of systems with completely non-interactive visualizations results in a bad experience for the user.

In VR, a user is fully closed-off from the real world and only sees the interactive 3D visualization as if this was the real world. Interactions with this world are mostly done using specific controllers that in many cases are tracked (and often visualized) in the virtualized world as well. Several types of VR systems are available nowadays, like the HTC Vive and the Oculus Rift.

In AR, the 3D visualization is usually projected onto (semi-)transparent glasses that allow a user to see the virtual, visualized world superimposed on the real-world. To the

user it appears like the visualizations are located in the real world. Examples of such systems are the Microsoft Hololens and the Magic Leap system.

The benefit of VR and AR visualizations over more traditional methods of visualization is that a user is fully immersed in the visualization and can experience the visualization as if it were the real world. This makes these systems very useful in simulation environments where a user is supposed to experience a simulated environment as if it were real. This is useful for training simulations like a welding simulator teaching someone how to make a good weld, or a surgical simulator that can be used by a physician to train an operation.

AR systems can be used in simulations where a user needs to be assisted with something that needs to be done in the real world. For example, an AR system could indicate to an engineer what part of a machine in need of service needs to be replaced, or how a replacement should be done. On the other hand, a physician performing a complex operation could be assisted in AR with planning information or a live overlay of a CT or MRI scan made earlier.